AD A039064

RADC-TR-77-110
Technical Report
March 1977

NUMERICAL CALCULATION OF MICROTHERMAL TEMPORAL SPECTRA

The Ohio State University

Approved for public release; distribution unlimited.

Sponsored by
Defense Advanced Research Projects Agency (DoD)
ARPA Order No. 1279

The views and conclusions contained in this document are those of the authors and should not be interpreted as necessarily representing the official policies, either expressed or implied, of the Defense Advanced Research Projects Agency or the U. S. Government.

AU NO.
DDC FILE COPY

DDC
RECEIVED
MAY 6 1977
D

ROME AIR DEVELOPMENT CENTER
AIR FORCE SYSTEMS COMMAND
GRIFFISS AIR FORCE BASE, NEW YORK 13441

This report has been reviewed by the RADC Information Office (OI) and is releasable to the National Technical Information Service (NTIS). At NTIS it will be releasable to the general public including foreign nations.

This report has been reviewed and is approved for publication.

APPROVED: James W Cusack

JAMES W. CUSACK
Project Engineer

Do not return this copy. Retain or destroy.

ACCESSION for
NTIS White Section
DDC Buff Section
UNANNOUNCED
JUSTIFICATION
BY
DISTRIBUTION/AVAILABILITY CODES
Dist. AVAIL. and/or SPECIAL
A

NUMERICAL CALCULATION OF MICROTHERMAL TEMPORAL SPECTRA

D. D. Duncan
S. A. Collins, Jr.

Contractor: The Ohio State University,
Contract Number; F30602-76-C-0058
Effective Date of Contract: 1 July 1975
Contract Expiration Date: 30 September 1977
Short Title of Work: Numerical Calculation of Microthermal Temporal Spectra
Program Code Number: 5E20
Period of Work Covered: Jul 75 - Jan 76

Principal Investigator: S. A. Collins, Jr.
Phone: 617 422-6077
Project Engineer: James W. Cusack
Phone: 315 330-3145

Approved for public release;
distribution unlimited.

This research was supported by the Defense Advanced Research Projects Agency of the Department of Defense and was monitored by James W. Cusack (OCSE), Griffiss AFB NY 13441 under Contract F30602-76-C-0058.

DDC
RECEIVED
MAY 6 1977
D

UNCLASSIFIED

SECURITY CLASSIFICATION OF THIS PAGE (When Data Entered)

REPORT DOCUMENTATION PAGE

READ INSTRUCTIONS BEFORE COMPLETING FORM

1. REPORT NUMBER: RADC-TR-77-110	2. GOVT ACCESSION NO.
3. RECIPIENT'S CATALOG NUMBER	
4. TITLE (and Subtitle): NUMERICAL CALCULATION OF MICROTHERMAL TEMPORAL SPECTRA	5. TYPE OF REPORT & PERIOD COVERED: Interim Report Jul 75 - Jan 76
6. PERFORMING ORG. REPORT NUMBER: ESL-4232-3	
7. AUTHOR(s): D. D. Duncan; S. A. Collins, Jr.	8. CONTRACT OR GRANT NUMBER(s): F30602-76-C-0058; ARPA Order - 1279
9. PERFORMING ORGANIZATION NAME AND ADDRESS: The Ohio State University/ElectroScience Laboratory, Department of Electrical Engineering, Columbus OH 43212	10. PROGRAM ELEMENT, PROJECT, TASK AREA & WORK UNIT NUMBERS: 62301E; 12790508
11. CONTROLLING OFFICE NAME AND ADDRESS: Defense Advanced Research Projects Agency, 1400 Wilson Blvd, Arlington VA 22209	12. REPORT DATE: March 1977
	13. NUMBER OF PAGES: 39 (34 Repo)
14. MONITORING AGENCY NAME & ADDRESS(if different from Controlling Office): Rome Air Development Center (OCSE), Griffiss AFB NY 13441	15. SECURITY CLASS. (of this report): UNCLASSIFIED
	15a. DECLASSIFICATION/DOWNGRADING SCHEDULE: N/A

16. DISTRIBUTION STATEMENT (of this Report)

Approved for public release; distribution unlimited.

17. DISTRIBUTION STATEMENT (of the abstract entered in Block 20, if different from Report)

Same

402 251

18. SUPPLEMENTARY NOTES

RADC Project Engineer:
James W. Cusack (OCSE)

19. KEY WORDS (Continue on reverse side if necessary and identify by block number)

Microthermal fluctuations
Spectrum estimation
FFT
Digital processing

20. ABSTRACT (Continue on reverse side if necessary and identify by block number)

This report presents and discusses several accepted techniques employed in the digital estimation of power spectra. These methods were applied to the calculation of power spectra of microthermal fluctuations. Discussed herein are such topics as preliminary data management, data windows, pre-whitening and post-darkening, confidence intervals, digital filtering, and the use of the fast Fourier transform algorithm (FFT).

DD FORM 1 JAN 73 1473 EDITION OF 1 NOV 68 IS OBSOLETE

UNCLASSIFIED

SECURITY CLASSIFICATION OF THIS PAGE (When Data Entered)

PREFACE

This report, Ohio State University Research Foundation Report Number 4232-3, was prepared by The Ohio State University ElectroScience Laboratory, Department of Electrical Engineering at Columbus, Ohio. Research was conducted under Contract F30602-76-C-0058 (Project PR-A-1639). Mr. James W. Cusack, RADC (OCSE), of Rome Air Development Center, Griffiss Air Force Base, New York, is the Project Engineer.

CONTENTS

SECTION I

MICROTHERMAL SPECTRAL EXAMINATION

This report is concerned with the estimation of power spectra of microthermal fluctuations. It represents work directed at verifying spectra being routinely obtained from microthermal data recorded using high-flying aircraft. The material within this report is not intended to represent new and unique research in the field of digital signal processing, but rather to document and discuss the various well accepted techniques.

The microthermal fluctuations are important because they give information on spatial refractive index fluctuations which is necessary to the calculation of the behavior of light beams propagating to and from high-flying aircraft. During 1974 and 1975 many such spectra were obtained at Kirtland Air Force Base to provide a heretofore unavailable data base for such calculations. The calculations presented here were performed as a routine check on these spectra and the procedures used to obtain them.

The microthermal fluctuation data are obtained using a platinum-wire microthermal sensor mounted near the front or top on an aircraft fuselage and sufficiently removed from the surface to be outside the aircraft boundary layer. The data are recorded on FM analog tape in sections roughly two minutes in duration. Typically six to twelve such runs might be recorded in one flight. The data are then possibly filtered, digitized, and computer processed to obtain the temporal spectra. The spectra obtained here check on the data processing portion of the effort, repeating the digitization and computer processing.

Section II of this report contains a discussion of the preliminary data management including digitization rates, scaling and the removal of some spikes that were found in the analog record. Sections III and IV contain the details of the procedures for obtaining the spectra. The spectra were divided into frequency regions. Section III contains the details of the basic processing procedure. These were used directly in the highest frequency region. The basic procedure includes multiplying by data windows, pre-whitening/post-darkening, ensemble averaging, and the calculation of confidence intervals. In Section IV the additional procedures of smoothing and decimation, necessary for extending the spectrum to lower frequency ranges, are presented. The results of the combined high and low frequency procedures are presented in Section V. Section V also contains a comparison with the spectrum obtained previously at Kirtland Air Force Base. Section VI gives some thoughts on procedures suggested to improve spectral resolution and reliability.

SECTION II

DIGITIZATION AND PRELIMINARY PROCESSING

In this section we present a discussion of the sampling rate and a discussion of one other problem, the occurence of spikes in the primary data tape.

To be thorough we elected to determine our own digitization rate. The full bandwidth of the electronics was 20 KHz. To achieve at least this sampling frequency with the available 500 Hz A-D converter, we played-back the tape at a speed reduced from 30 IPS by a factor of 64, i.e., at a tape speed of 15/32 IPS. At this tape speed the Nyquist rate corresponding to our system bandwidth is 312.5 Hz.

Calibration of the data was accomplished by means of a $\pm$.15°C 100 Hz square wave recorded on the leading edge of the tape. Several cycles of this reference square wave were digitized along with approximately 2 minutes of data. In addition to calibrating the magnitude of the temperature fluctuations, inspection of the digitized version of the square wave enabled the accurate calculation of the sampling rate. This precise value of the equivalent sampling rate was 30.65 KHz. Inspection of the digitized microthermal data revealed several periods with severe spiking. Such spiking is exemplified by Figure 1, which represents 33.5 msec. of data. (The straight line represents the average temperature.) The spiking in general consisted of from two to five very narrow ($\sim$130 μsec) pulses spaced approximately 8 msec. apart. The inter-group spacing appeared to be random. Since inclusion of these spikes in our spectral calculations would decrease the reliability of our results, they were eliminated by a simple linear interpolation between data points on either side of the spikes. The same time span of data shown in Figure 1 is again shown in Figure 2 with the spikes removed by the interpolation scheme.

This concludes our discussion of the preliminary processing of the microthermal data including digitization, scaling and spike removal. The next section outlines the techniques employed in the high-frequency analysis.

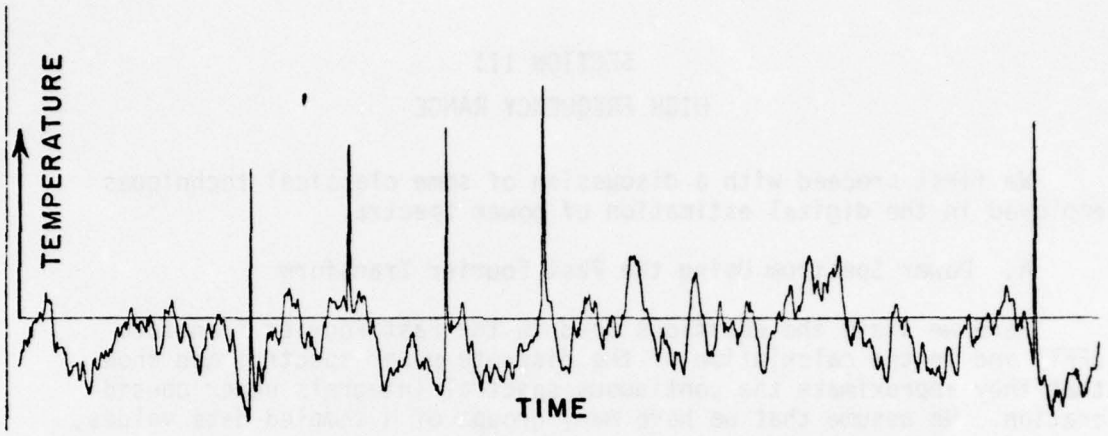

Figure 1. Time trace of raw microthermal data.

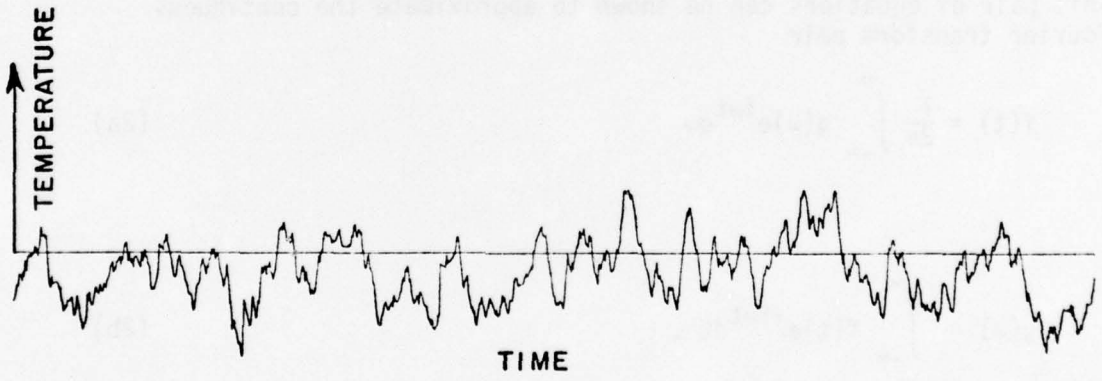

Figure 2. Time trace of microthermal data with spikes removed.

SECTION III

HIGH FREQUENCY RANGE

We first proceed with a discussion of some classical techniques employed in the digital estimation of power spectra.

A. Power Spectrum Using the Fast Fourier Transform

Here we state the equations used in the Fast Fourier Transform (FFT) and in the calculation of the discrete power spectrum and show that they approximate the continuous spectral integrals under consideration. We assume that we have many groups of N sampled data values, sampled at intervals of t_o.

The equations implemented by the FFT algorithm are

$$X(L) = \sum_{K=1}^{N} C(K)\, e^{i\frac{2\pi}{N}(K-1)(L-1)} \tag{1a}$$

$$C(K) = \frac{1}{N} \sum_{L=1}^{N} X(L) e^{-i\frac{2\pi}{N}(K-1)(L-1)} . \tag{1b}$$

This pair of equations can be shown to approximate the continuous Fourier transform pair

$$f(t) = \frac{1}{2\pi} \int_{-\infty}^{\infty} g(\omega) e^{i\omega t} d\omega \tag{2a}$$

$$g(\omega) = \int_{-\infty}^{\infty} f(t) e^{-i\omega t} dt . \tag{2b}$$

This is accomplished using the substitutions

$$L = L' + \frac{N}{2} \tag{3a}$$

$$F(L't_o) = X(L' - \frac{N}{2})$$

$$G(2\pi K/Nt_o)e^{-i\pi(K-1)} = Nt_oC(K) \tag{3c}$$

and by changing the limits on K to (1- N/2, N/2) which can be done because C(K) is periodic, C(K) = C*(N-K+2). These substitutions allow Equations (1) to be written in the form

$$F(Lt_o) = \frac{1}{2\pi} \sum_{K=1-\frac{N}{2}}^{\frac{N}{2}} G(K2\ /Nt_o)e^{i\frac{2\pi}{Nt_o}(K-1)(L-1)t_o} \frac{2\pi}{Nt_o} \tag{4a}$$

$$G(2\pi K/Nt_o) = \sum_{L'=1-\frac{N}{2}}^{\frac{N}{2}} F(L't_o)e^{-\frac{2\pi}{Nt_o}(K-1)(L'-1)t_o} t_o. \tag{4b}$$

The substitutions in Equations (3) serve two purposes. They allow the identfication of the correspondence between the discrete and continuous variables, as in the following expressions;

$$t \sim Nt_o \tag{5a}$$

$$dt \sim t_o \tag{5b}$$

$$\omega \sim 2\pi K/Nt_o \tag{5c}$$

$$d\omega \sim 2\pi/Nt_o \tag{5d}$$

$$f(t) \sim F(L't_o) \equiv X(L') \tag{5e}$$

$$g(\omega) \sim G(2\pi K\ /Nt_o)e^{i\pi(K-1)} \equiv Nt_oC(K). \tag{5f}$$

The second purpose is for completeness. It is to shift the summation limits to make them symmetric. This is done in the frequency domain by changing the summation limits from (1,N) to (1-N/2, N/2) (allowed since the representation is periodic) and by translating the data string to make it symmetric.

It is assumed that the data is sampled sufficiently rapidly so that the summations accurately represent the respective integrations.

The autocorrelation $R(Lt_o)$, and the power spectral density, $S(K2/Nt_o)$ are defined respectively in Equations (6). The angular brackets indicate ensemble averaging.

$$R(Lt_o) = \langle F(It_o)F^*((I+L-1)t_o)\rangle \tag{6a}$$

$$= \frac{1}{2\pi} \sum_{1-N/2}^{N/2} S(K2/Nt_o) e^{i\frac{2\pi}{Nt_o}(K-1)(L-1)} \frac{2\pi}{Nt_o} \tag{6b}$$

These are to be compared with the corresponding equations for the continuous case:

$$R(t_1,t_2) = \langle f(t_1)f^*(t_2)\rangle \tag{7a}$$

$$R(t_1,t_2) = \frac{1}{2\pi} \int_{-\infty}^{\infty} W(\omega) e^{i\omega(t_1-t_2)} . \tag{7b}$$

We also have for the continuous case,

$$\langle g(\omega_1)g^*(\omega_2)\rangle = W(\omega_1)\delta(\omega_1-\omega_2) . \tag{7c}$$

Clearly the spectral density, $W(\omega)$ corresponds to $S(K2\pi/Nt_o)$ in the discrete case.

The power spectral density, S, for the discrete case is related to the transform of the data, C(K) by Equation (8).

$$Nt_o\langle C(K_1 2\pi/Nt_o)C^*(K_2 2\pi/Nt_o)\rangle e^{-i\pi(K_1-K_2)} = \delta_{K_1K_2} S(K2\pi/Nt_o) \tag{8}$$

Equation (8) is the discrete counterpart of the continuous form in Equation (7c). Thus for any single data transform we take for computational purposes

$$S(K2\pi/Nt_o) = T|C(K2\pi/Nt_o)|^2 \tag{9}$$

where

$$T = Nt_o \tag{10}$$

We note that there are only N/2 unique values for the spectrum, $S(k2\ /Nt_o)$. This follows because $S(K2\pi/Nt_o)$ is symmetric about zero frequency. Thus the frequency dynamic range is π/t_o, covering the range $(2\pi/Nt_o, \pi/t_o)$.

B. Trend Removal

To improve our estimates of the very low frequency components of our data, it is beneficial to remove the DC and linear trends [4] before calculating the power spectrum.

The suposition that the data of interest are modulated by a linear trend is expressed as;

$$x_i = \hat{\beta}_o + \hat{\beta}_1 t_i + x_i', \tag{11a}$$

where the x_i are the original data, $\hat{\beta}_o$ and $\hat{\beta}_1$ are respectively estimates of the DC and linear trend, and the x_i' are the data of interest. It is easily shown [1] that for a minimum mean square error fit,

$$\hat{\beta}_1 = \frac{N\Sigma t_i x_i - \Sigma t_i \Sigma x_i}{N\Sigma t_i^2 - (\Sigma t_i)^2} \tag{11b}$$

$$\hat{\beta}_o = \frac{1}{N}(\Sigma x_i - \hat{\beta}_1\ t_i)\ . \tag{11c}$$

Without loss of generality we can assume $t_i=(i-1)$. In this case Equations (11) simplify somewhat to yield,

$$\hat{\beta}_1 = \frac{12}{N(N^2-1)} \left[\Sigma(i-1)x_i - \frac{(N-1)}{2} \Sigma x_i\right] \tag{12a}$$

$$\hat{\beta}_0 = \frac{1}{N} \left[\Sigma x_i - \hat{\beta}_1 \frac{N(N-1)}{2}\right] . \tag{12b}$$

The data of interest are then given by

$$x_i' = x_i - \hat{\beta}_0 - \hat{\beta}_1(i-1) . \tag{13}$$

The reason for subtracting linear trends is to improve low-frequency estimates when the data string is not sufficiently long to give information about the lowest frequencies. Thus a linear trend could be part of a sine wave with period longer than the data duration. The effect of a trend is to augment the values of the lowest few harmonics by adding in the Fourier series spectrum of a linear waveform thus giving incorrect values. The existence of the lower frequencies can be indicated by the shape of the lower frequency portion of the spectrum. If the spectral values continue to rise as the frequency decreases right down to the lowest harmonic, then the existence of even lower frequencies would seem quite possible.

C. Hanning and Compensation for Non-Unity Energy

The use of the finite discrete Fourier transform pair (Equations (3a,b)) implies that we are looking at a finite section of an infinite string of data [7]. That is, we are viewing our data through a rectangular data window of unity height and length T. Multiplication of our data by this window results in the true spectrum being convolved with a sin(x)/x function*. Since this function has significant sidelobes, we wish to somehow alter our rectangular window so that the resulting convolution is with a function with significantly lower side lobes. Such a data window commonly known as the Hanning window [4] is given by

$$\frac{1}{2}\left[1 + \cos\frac{(L-1-N/2)\pi}{N/2}\right] . \tag{14}$$

*This error is often referred to as leakage.

Equivalent to multiplying our data by this window and transforming, is simply calculating [2] in the frequency domain

$$C(K) \leftarrow \begin{cases} \frac{1}{2} C_1 - \frac{1}{2} \mathrm{Re}(C_2) \; ; \; K=1 \\ -\frac{1}{4} C_{K-1} + \frac{1}{2} C_K - \frac{1}{4} C_{K+1} ; \; K=2,3,\cdots, \frac{N}{2} \end{cases} \tag{15}$$

Note that by use of our data window as in Equation (14), we have decreased the energy in our original data. Therefore to obtain an unbiased estimate of the true power spectrum [3], we require that the Hanned estimation on the right hand side of Equation (9) be multiplied by 8/3. See Appendix A for a demonstration of this factor.

D. Pre-Whitening and Post-Darkening

We next consider the problem of estimating the harmonics of a spectrum which has a large dynamic range, i.e., one which is steeply sloping. Recall from Section C that the spectrum we calculate is really the true spectrum convolved with the transform of our data window. If the true spectrum is steeply sloping even though the side lobes of the transform of the data window are small, the product of the harmonics of the side lobe and the off-center harmonic (which is much greater than the center harmonic) of the true spectrum may be comparable to the estimate of the center harmonic. Therefore to reduce this problem, we resort to the technique of pre-whitening [4] which effectively evens out the true spectrum. Such a pre-whitening scheme is implemented by calculating

$$x_i \leftarrow \begin{cases} x_i - \alpha \, x_{i-1} ; \; i=2,3,\cdots,N \\ \\ x_i \qquad\qquad ; \; i=1, \end{cases} \tag{16}$$

where α is the pre-whitening parameter. Some a priori knowledge of the general shape and dynamic range of the true power spectrum is needed to choose a value for α. Use of expression (16) results in the true power spectrum being multiplied [4] by

$$\left| 1-\alpha \, e^{\,i \frac{2\pi(L-1)}{N}} \right|^2 . \tag{17}$$

This function is shown plotted in Figure 3 for several representative values of α. For the high frequency range, $\alpha = 0.975$ seemed to be a good choice for our data.

So to summarize, our procedure for power spectrum estimation amounts to;

1) removing DC and linear trends (Equations (12) and (13))
2) prewhitening (expression (16))
3) calculating the voltage spectrum C(K) (Equation (3b))
4) hanning the spectral components C(K) (expression (15))
5) calculating the power spectral harmonics S(K) (Equation (3a))
6) compensating for non-unity energy in the data window by multiplying the S(K) by 8/3
7) post-darkening by dividing the power spectral estimates S(K) by expression (17).

E. Ensemble Averaging, Confidence Intervals

We now come to the question of how adequately our spectra estimate the true power spectrum. If we assume we have calculated several spectra (of successive data strings of period T) then assuming that all the data are from a random stationary process, we can average at each spectral harmonic [5], over all the spectral realizations. That is if the ith harmonic of the jth spectral realization is denoted as S_{ij}, then our average spectrum will be given by

$$\hat{S}_i = \frac{1}{L} \sum_{j=1}^{L} S_{ij} \tag{18}$$

where $\hat{S}_i$ denotes the estimate of the ith harmonic of the true spectrum S_i.

If we now assume that the original data were samples from a gaussian random process with zero mean and power spectrum S_i then the statistic

$$Y = \frac{2L\hat{S}_i}{S_i} \tag{19}$$

has an approximate chi-square distribution [6] with 2L degrees of freedom ($\chi^2(2L)$). The factor of 2 arises because S_i is the modulus of a complex random variable C_i (2 degrees of freedom).

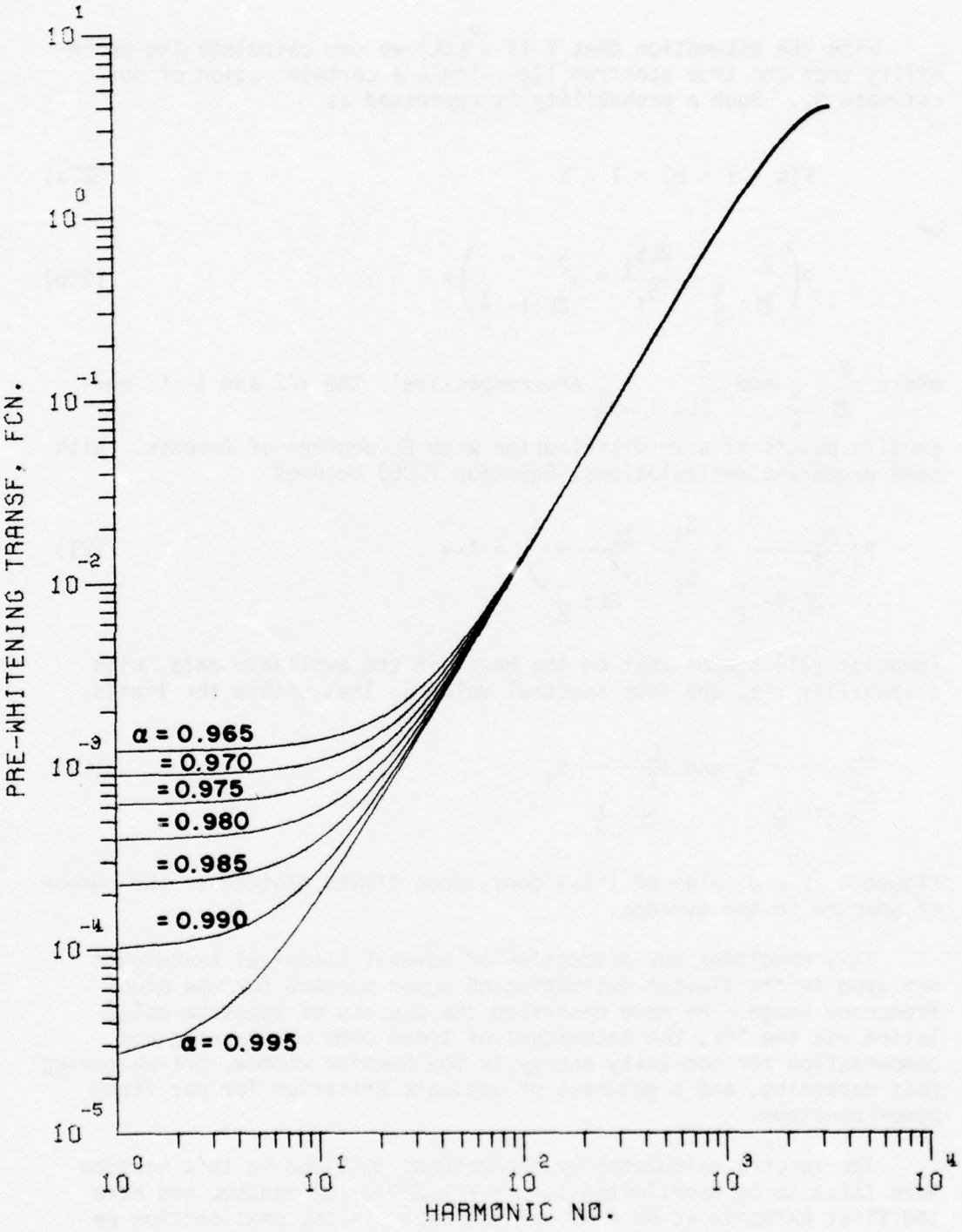

Figure 3. Pre-whitening power transfer function for various values of the pre-whitening parameter α.

With the assumption that Y is $\chi^2(2L)$ we can calculate the probability that the true spectrum lies within a certain region of our estimate S_i. Such a probability is expressed as

$$P(a < Y < b) = 1 - \gamma \tag{20a}$$

or

$$P\left(\chi^2_{2L;\frac{\gamma}{2}} < \frac{2L\hat{S}_i}{S_i} < \chi^2_{2L;1-\frac{\gamma}{2}}\right) = 1 - \gamma \tag{20b}$$

where $\chi^2_{2L;\frac{\gamma}{2}}$ and $\chi^2_{2L;1-\frac{\gamma}{2}}$ are respectively the $\gamma/2$ and $1-\gamma/2$ percentile points of a χ^2 distribution with 2L degrees of freedom. With some algebraic manipulations, Equation (20b) becomes

$$P\left(\frac{2L}{\chi^2_{2L;1-\frac{\gamma}{2}}} < \frac{S_i}{\hat{S}_i} < \frac{2L}{\chi^2_{2L;\frac{\gamma}{2}}}\right) = 1-\gamma \ . \tag{21}$$

Equation (21) states that on the basis of the available data, with probability $1-\gamma$, the true spectral value S_i lies within the limits

$$\frac{2L}{\chi^2_{2L;1-\frac{\gamma}{2}}}\hat{S}_i \text{ and } \frac{2L}{\chi^2_{2L;\frac{\gamma}{2}}}\hat{S}_i \ . \tag{22}$$

Figure 4 is a display of these confidence limits plotted vs the number of spectra in the average.

This concludes our discussion of several classical techniques employed in the digital estimation of power spectra for the high-frequency range. We have described the process of spectrum calculation via the FFT, the techniques of trend removal, hanning and compensation for non-unity energy in the hanning window, pre-whitening/post-darkening, and a goodness of estimate criterion for our final power spectrum.

The spectra calculated by the methods outlined in this section were taken to be bandlimited to $\omega = \pm 9.629 \times 10^4$ rad/sec and have the first harmonic at $\Delta\omega = 47.017$ rad/sec. In the next section we will give a procedure for estimating frequencies lower than 47 rad/sec.

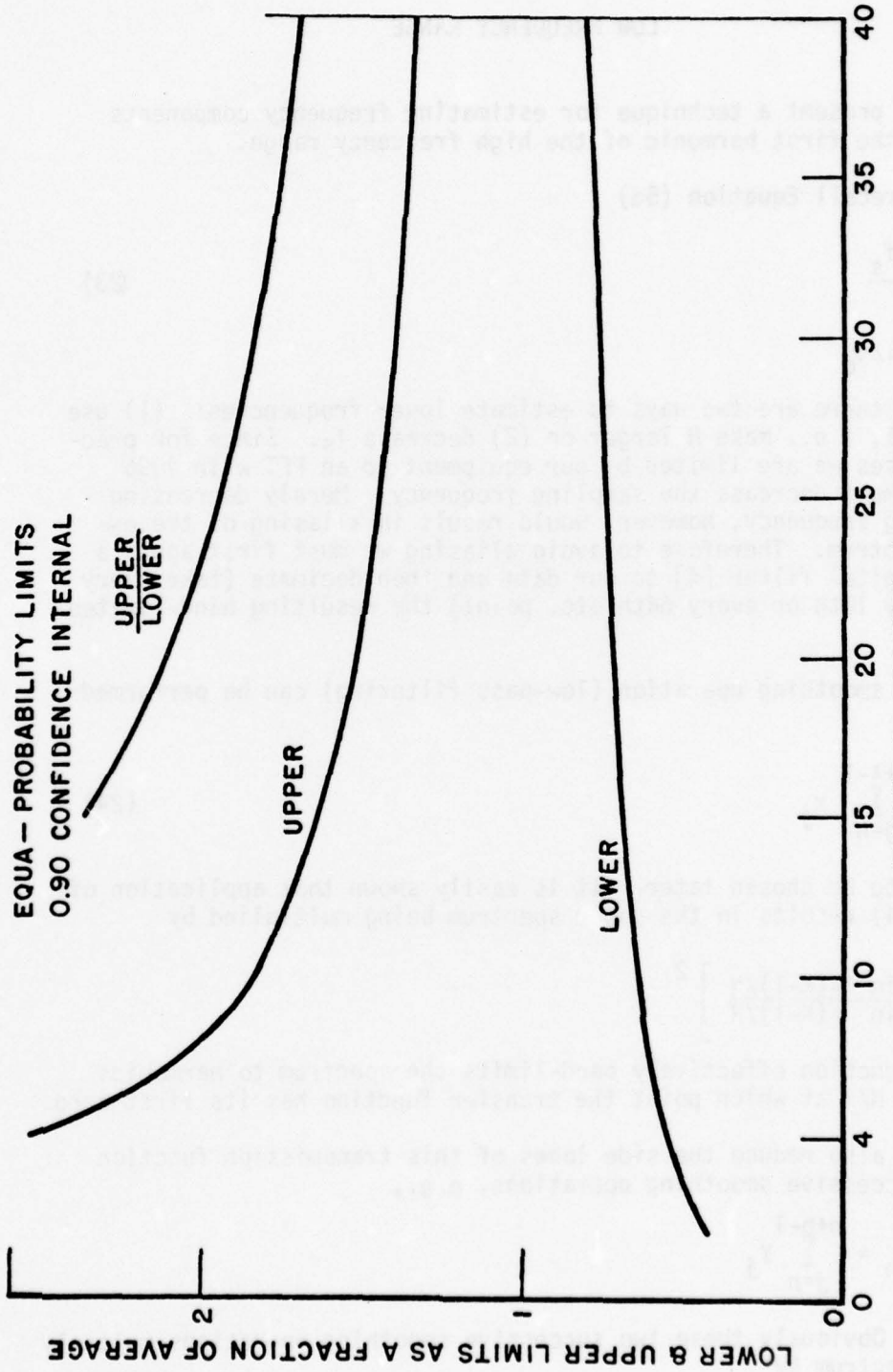

Figure 4. Normalized confidence limits as a function of the number of ensemble members.

SECTION IV

LOW FREQUENCY RANGE

We now present a technique for estimating frequency components lower than the first harmonic of the high frequency range.

If we recall Equation (5d)

$$\Delta\omega = \frac{2\, f_s}{N} \tag{23}$$

where $f_s = 1/t_o$

we see that there are two ways to estimate lower frequencies: (1) use a larger FFT, i.e., make N larger or (2) decrease f_s. Since for practical purposes we are limited by our equipment to an FFT with 4096 points, we must decrease the sampling frequency. Merely decreasing the sampling frequency, however, would result in aliasing of the estimated spectrum. Therefore to avoid aliasing we must first apply a low-pass digital filter [4] to our data and then decimate (take every 4th or every 10th or every 64th etc. point) the resulting band-limited data.

Such a smoothing operation (low-pass filtering) can be performed as

$$Y_n = \sum_{j=n}^{n+\ell-1} x_j \tag{24}$$

where ℓ is to be chosen later. It is easily shown that application of Equation (24) results in the power spectrum being multiplied by

$$\left[\frac{\sin \ell\pi(K-1)/N}{\sin \pi(K-1)/N}\right]^2$$

This function effectively band-limits the spectrum to harmonics one through N/ℓ at which point the transfer function has its first zero.

We may also reduce the side lobes of this transmission function by using successive smoothing operations, e.g.,

$$Z_n = \sum_{j=n}^{n+p-1} Y_j$$

where $p \neq \ell$. Obviously these two successive smoothing operations multiply the true spectrum by

$$\left[\frac{\sin \ell\pi(K-1)/N}{\sin \pi(K-1)/N}\right]^2\left[\frac{\sin p\pi(K-1)/N}{\sin \pi(K-1)/N}\right]^2 \quad . \tag{25}$$

With the smoothing operation thus accomplished we can then decimate our data without folding harmonics N/ℓ through $N/2 - 1$ onto harmonics zero through $N/\ell - 1$.

Then one can go on with the general procedure outlined previously. After performing these calculations, the resulting spectra are then simply divided by expression (25).

$$\left[\frac{\sin \ell\pi(K-1)/(nN)}{\sin \pi(K-1)/(nN)}\right]^2 \left[\frac{\sin p\pi(K-1)/(nN)}{\sin \pi(K-1)/(nN)}\right]^2 \quad , \tag{26}$$

where n is the decimation factor. This division operation deserves one word of caution: Division by the small magnitude of the filtering transfer function near the high frequency end of the pass-band emphasizes the effects of noise. Therefore these last few high frequency estimates should be discounted.

For the spectra calculated herein we chose to smooth successively by groups of 7 and 8. The power spectrum of these smoothing operators is shown in Figure 5. With the smoothing thus accomplished, we then decimated by 4, i.e., we kept only 1/4 the number of points. Figure 5 also shows the resulting aliasing. Going back to Equation (4) of the previous section we see that we have decreased the harmonic spacing (and the bandwidth) by a factor of four.

The advantage of this smoothing and decimation technique is that one can repeat the operation many times. Thus we can estimate arbitrarily low (limited only by the total amount of data) frequencies.

Smoothing techniques as evidenced by Equation (24) are of a general class known as nonrecursive filtering. The more elegant recursive filtering employs a linear combination of the form

$$Y_n = \sum_{i=0}^{\ell} a_i x_{n+1} + \sum_{i=1}^{k} b_i Y_{n-i}.$$

With the proper choice of weights a_i and b_i this summation yields the digital analog of more sophisticated filters, e.g., Butterworth, Chebyshev. Reference 10 contains a comprehensive discussion of these techniques.

This ends the theoretical background for the estimation of micro-thermal fluctuation power spectra. In the next section we consider the selection of spectral ranges, i.e., data record lengths and decimation factors for the desired confidence intervals.

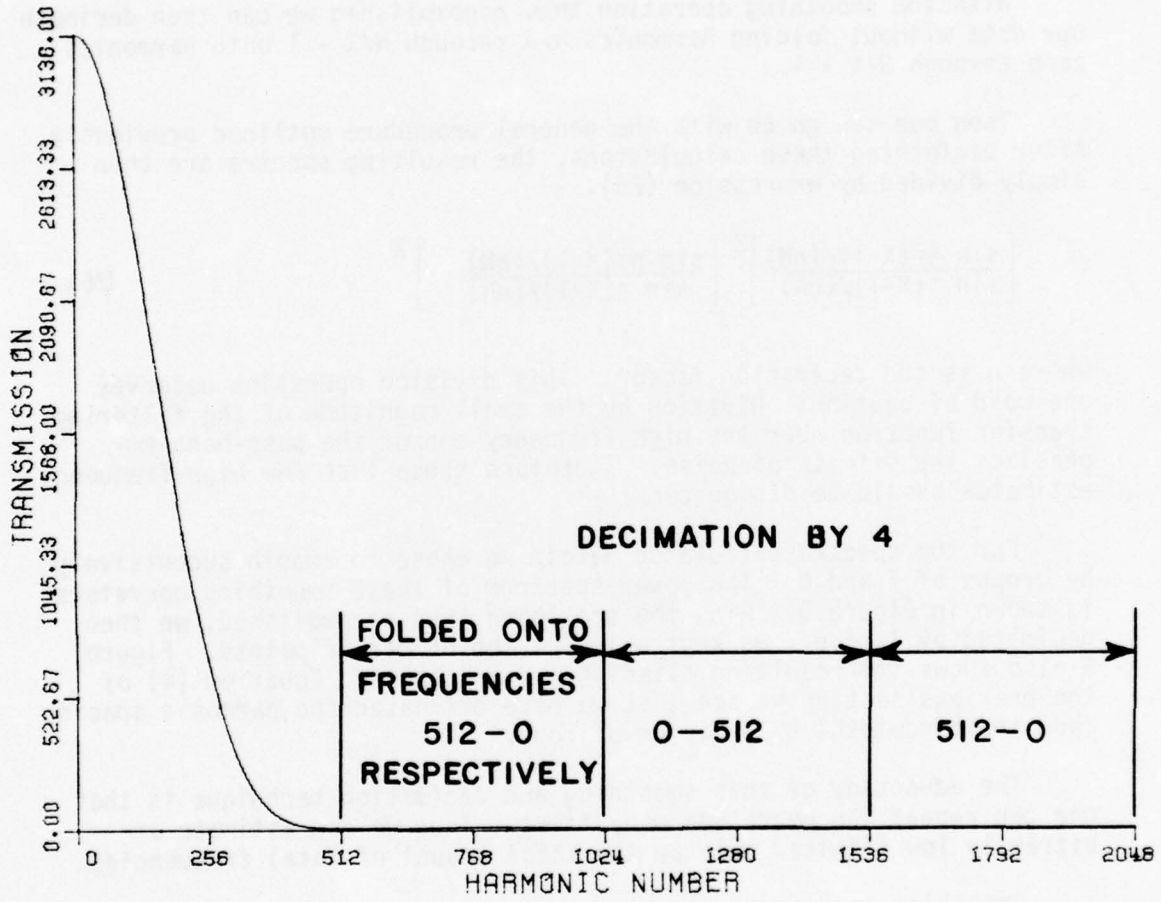

Figure 5. Power transfer function for smoothing by groups of 7 and 8.

SECTION V

SELECTION OF SPECTRAL RANGES

We now consider a question not mentioned previously. That is, given a very large amount of data how should it be divided in order to obtain the best spectra the most efficiently? This question is faced every time one analyzes a data sequence of more points than the largest available FFT. The answer determines the precision of the spectral estimates and the required computer time and must certainly be determined before starting the procedures of Sections III and IV. Here we present recommendations to assist in the solution of this problem for any particular case.

The result of the procedures described in this chapter is a composite spectrum covering several different ranges. These will be obtained from data sequences of different time durations. The higher the frequency, the shorter the time duration of data which is required. The data sequence for each spectral range is divided into sections, the spectrum is obtained for each, and all the spectra are averaged point by point to provide a statistically reliable estimate. For all but the highest frequency range the data sequence has been formed from the filtering and decimation procedures. The lowest frequency ranges will have no statistical averaging since the data have been decimated to the point where there are sufficient points for only a single FFT. As a rule there is reduced statistical reliability at the low frequency end of the spectrum.

We assume as starting information that the data sequence has a total time duration T_1, is bandlimited and has been digitized at a rate f_0, which is greater than or equal to the Nyquist rate. We expect as a final result a composite power spectrum with a lowest frequency around $1/T_1$ and a highest frequency of $f_0/2$. Four points should be considered in the section of spectral divisions:

1. the duration of the data sections for each spectral range
2. the number of spectra in the ensemble average for each spectral range
3. the factor by which to decimate
4. the treatment of the lowest frequency range.

The question of the duration required for the data sections will be considered first. The discussion is aimed primarily at the high frequency range, however it is applicable with the proper frequency scaling to all frequency ranges. The basic issue is whether to employ one large or several small FFT's. In the former case there would be fewer spectral ranges covering the same span of frequencies. The

answer depends upon the computer time required to perform large FFT's and a few filtering and decimation procedures as opposed to small FFT's and many filtering and decimation procedures. Since for many computers (as was the case here) the filtering and decimation procedure requires significant amounts of time, choosing the largest possible FFT gives the more efficient procedure. If the largest FFT required N points then the highest frequency range will span the frequencies f_o/N to $f_o/2$ as shown in Figure 6.

Now consider the question of statistical reliability. The desired precision is used in conjunction with Figure 4 which gives the ratio of confidence interval (normalized to the mean value) as a function of M, the number of spectra averaged. In addition it simplifies the decimation operation if M is chosen to be a power of 2. For our case M=32 seemed a good choice.

The next issue is the decimation rate. The guideline here is to decimate by a sufficient factor so that there is only a small overlap between the adjacent spectral ranges. An overlap of a factor of 8 or 16 seems to be reasonable. The factor of 8 gives at most eight points for comparison.

For decimation by a factor of 2^n the next to highest frequency range will run between $f_o/N2^n$ and $f_o/2(2)^n$, and after decimating m times the resulting frequency range will be between $f_o/N2^{nm}$ and $f_o/2(2)^{nm}$. The next to highest frequency range will require a data duration of $MN(2^n)/f_o$ seconds and after decimating m times the required data duration will be $MN(2^{nm})/f_o$ seconds. Finally we require that after m decimations each by a factor of 2^n we are left with exactly one record of N points.

The last point is the treatment of the lowest frequency range. This is important because in the low frequency ranges the duration of the individual sections is sufficiently long to reduce the number of sections, thus giving reduced statistical reliability. Indeed in the last range there will be only one section of duration T_1. The single spectrum yields minimum statistical confidence. For this frequency range confidence intervals may be improved by dividing the N remaining data points into several smaller sub-sections and performing a smaller FFT on each. This increases the lowest estimable frequency by a factor equal to the number of subsections. Therefore we see that as one attempts to estimate lower and lower frequencies (assuming the data is of limited extent) the confidence intervals must necessarily increase.

The low frequency problem can be minimized in many cases by choosing the digitizing frequency f_o so that there are exactly N data points after the final filtering/decimation operation and exactly M sections of N points each before the final smoothing and decimation operation. This requires that M, the number of sections averaged be

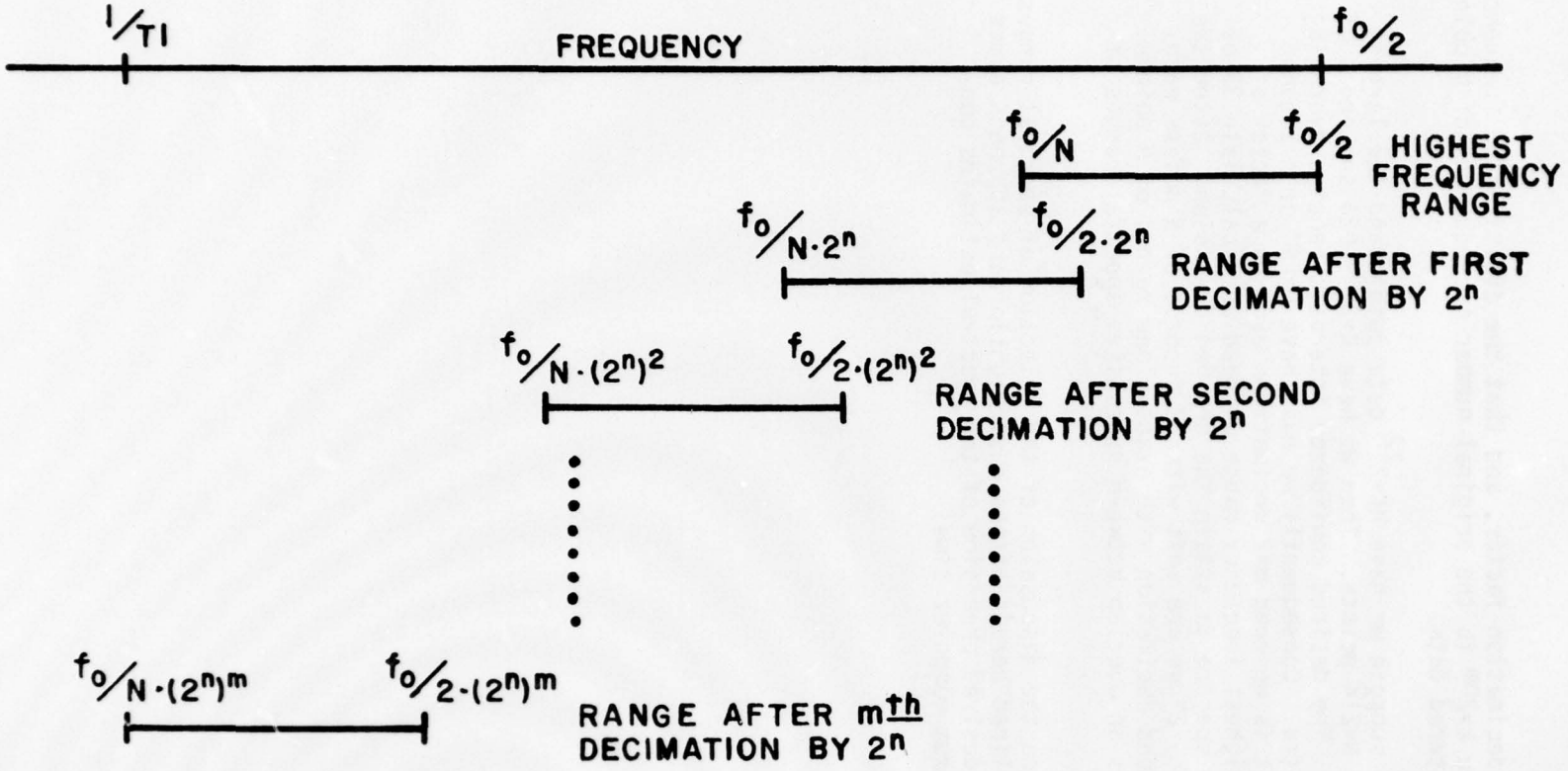

Figure 6. Frequency ranges for various decimation factors.

equal to 2^n, the decimation factor, and that the digitization frequency be $f_0=NK/T_1$, where $k=2^{nm}$ is the original number of sequences of N points each in the unfiltered data.

As an example suppose we have $NK=2^{22}$ data points and the largest available FFT has $N=2^{12}$ points. Then we have $K=2^{10}=1024$ sequences of 4096 points each. The desired confidence intervals require averaging over $M=2^5=32$ spectra. Consequently we must have $K=2^{nm}$ or $n=Log_2M=5$ so that m=2. That is we need m=2 decimations each by a factor of $2^n=32$. For the highest frequency range we need only calculate 32 of the possible 1024 spectra to attain the desired precision. After the first decimation by 2^5 we are left with 32 records of N points each, and after the second decimation with exactly one record of N points. This example gives an overlap between successive spectral ranges of $2^6=64$ points.

This completes the discussion of the selection of spectral ranges. The procedure outlined herein offers a straightforward approach aimed at providing the desired precision of the spectral estimates consistent with minimum computer time.

SECTION VI
RESULTS

We now present the results of the procedures which were outlined in Sections III, IV, and V.

Our results consist of several plots, each marked with a group number, a range number and an average over K files. The group number refers to a particular 8.36 second segment of data (of which there are 15). The range number n refers to the spectra calculated from data which have been decimated by a factor of $4^{(n-1)}$. Each file refers to a single 4096 point FFT, and the number K denotes the number of spectra averaged to produce the plot ($K=4^{(n-1)}$).

Plots 7 and 8 show the spectra calculated for ranges 1 and 2 respectively. We note the presence of the noise spikes. The first spike is at approximately 400 Hz, the second and third spikes are respectively 3rd and 5th harmonics of 400 Hz. The remaining spikes are all approximately harmonically related and as such can be discounted as legitimate data.

Plots 9 through 12 show the complete results for group 1. The noise spikes evident in ranges 1 and 2 have been removed. Note that in the regions of overlap between successive ranges there is very good agreement between spectral estimates.

Next, plots 13 through 15 are the same as plots three through five with the exception that we have also plotted the 90% confidence intervals.

Finally, Figures 16 are composites of the spectra from all frequency ranges averaged over the full 2.14 minutes. As a check on the spectrum calculated herein, the signal variance over the entire 2.14 minute run was estimated graphically from the spectrum of Figures 16-a and compared with the variance calculated from the raw data. The two estimates were found to differ by less than 2%.

By averaging spectra over the entire stretch of data we have obviously made the assumption that the process giving rise to the temperature fluctuations is wide-sense stationary. That this might be the case is indicated by the map shown in Figure 17.

The position and flight length during which the data were taken is indicated by the large black arrow. As can be seen, there are no large-scale geographical features in the area of data acquisition which would destroy the stationarity of the data. The map also shows surface features which could have a profound effect. Therefore this point should be checked on each data run until more is known about the effects of terrain features.

Figure 18 shows the spectrum obtained with the standard procedure used at Kirtland Air Force Base. The curve has been normalized so that the area under the curve is equal to $2\pi\sigma^2$ where σ^2 is the variance estimate obtained in this report. This normalization corrects for a discrepancy in spectral magnitudes. Comparison of Figures 16-a and 18 shows that the spectra agree quite closely.

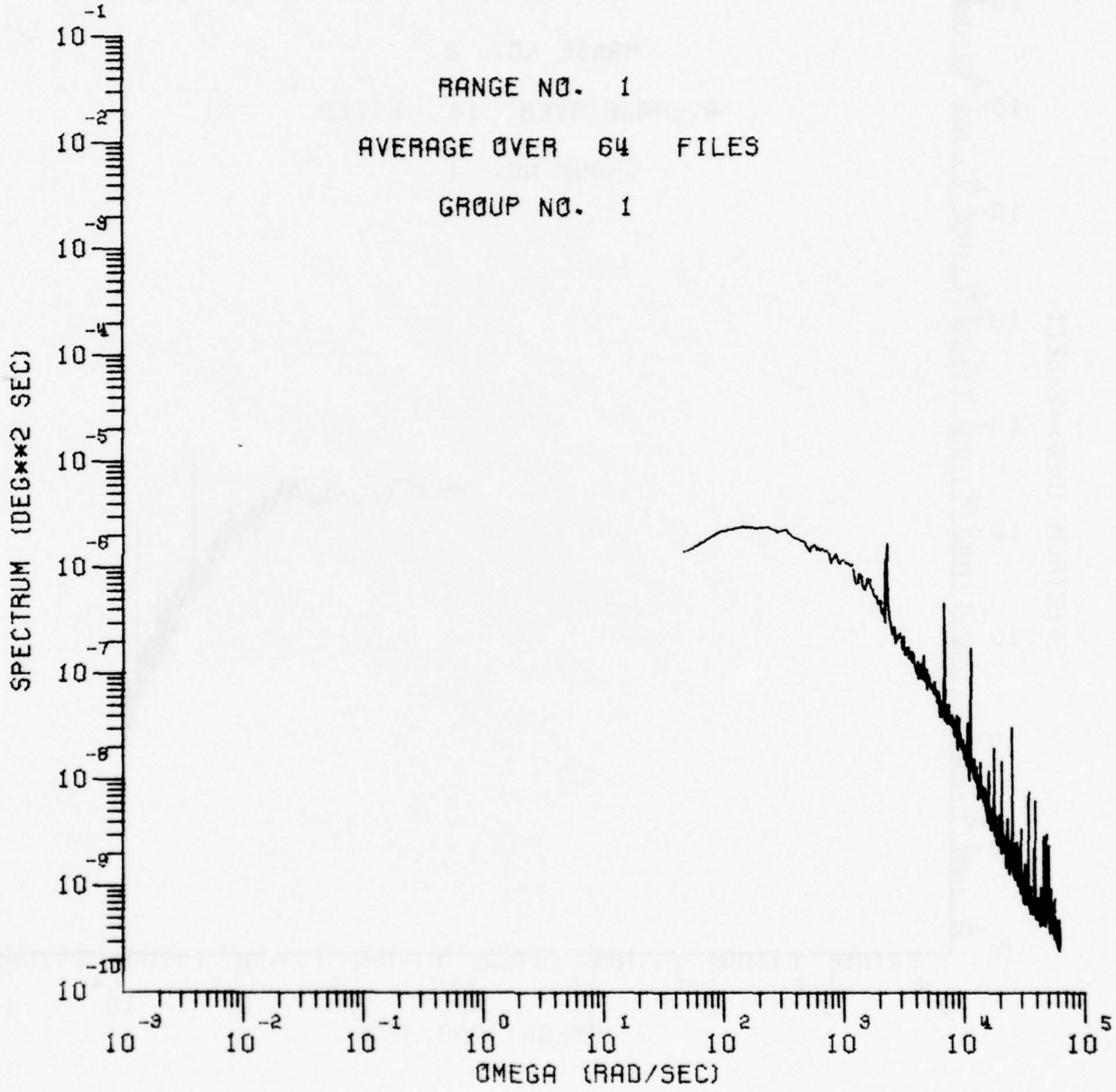

Figure 7. High frequency range spectrum.

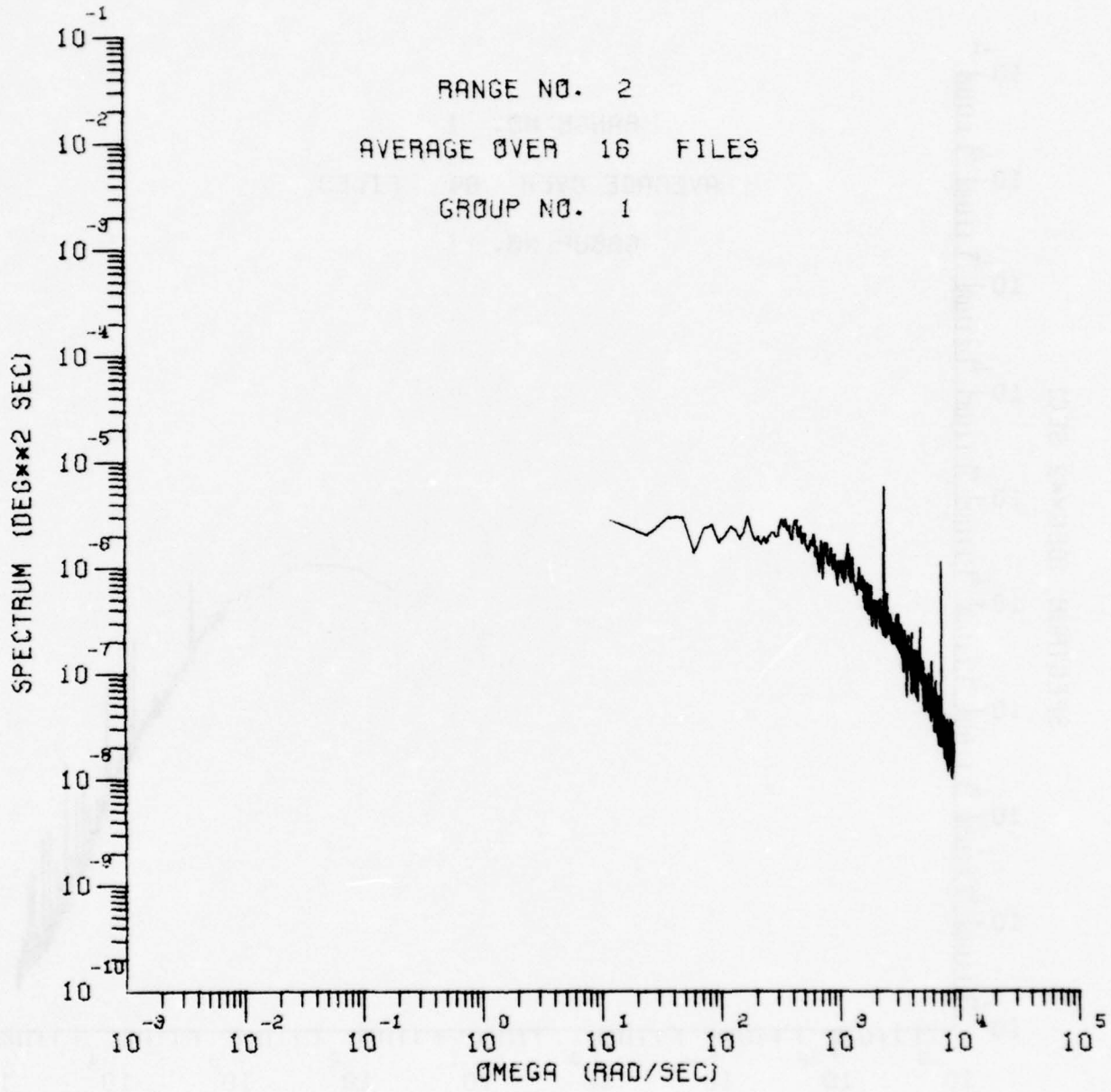

Figure 8. Second frequency range spectrum.

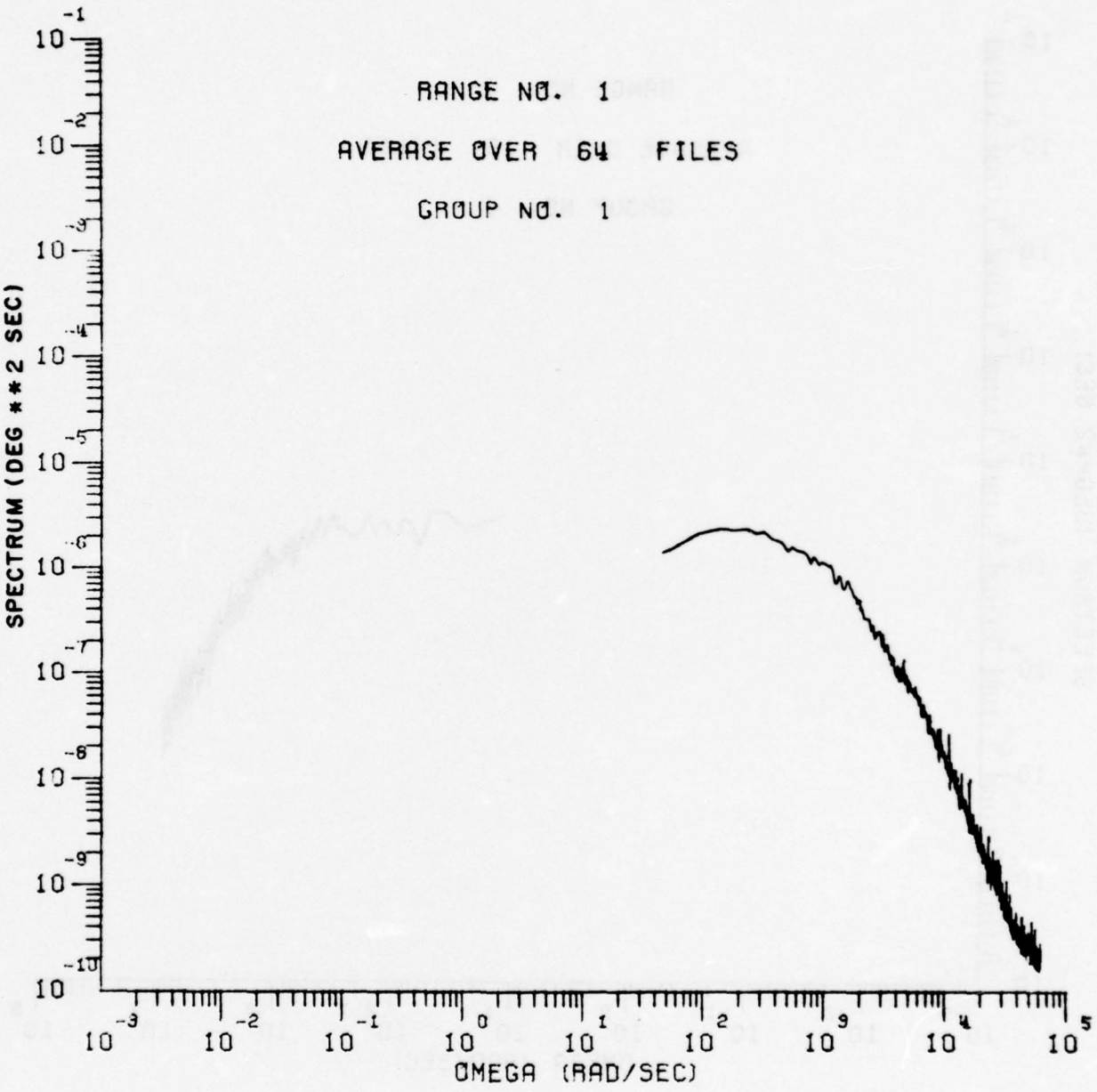

Figure 9. Same plot as in Figure 7 with frequency spikes removed.

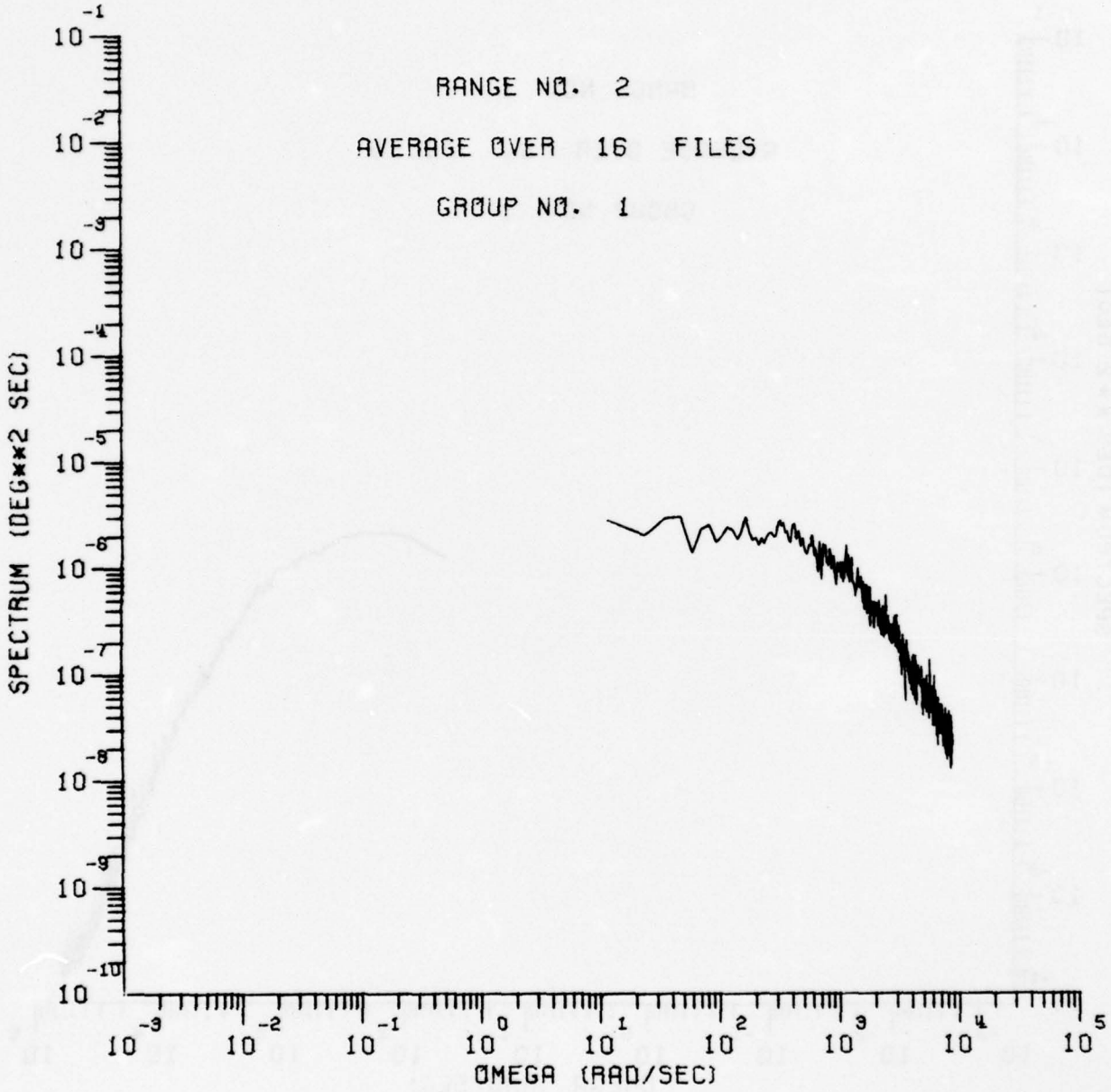

Figure 10. Same plot as in Figure 8 with frequency spikes removed.

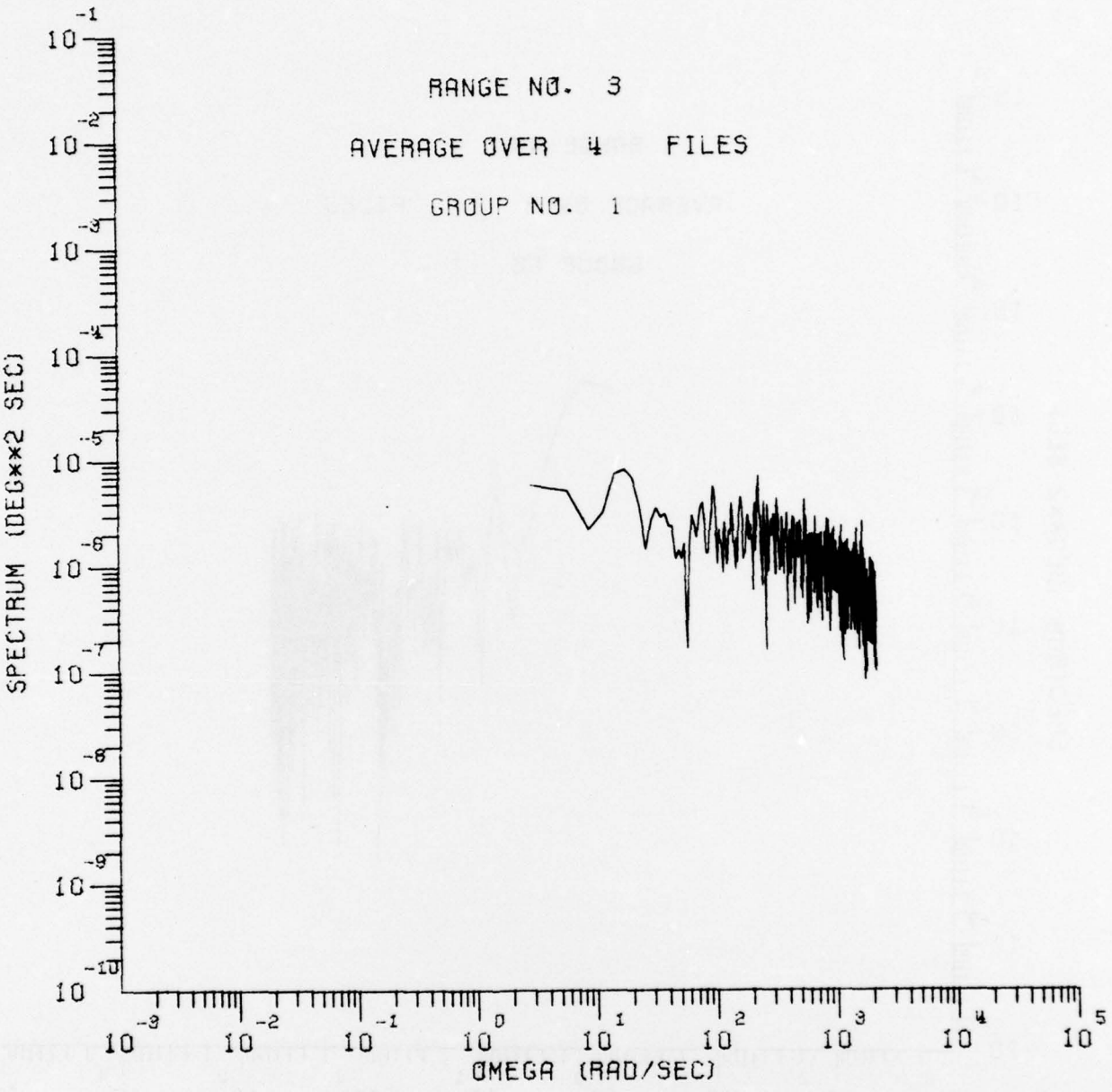

Figure 11. Third frequency range spectrum.

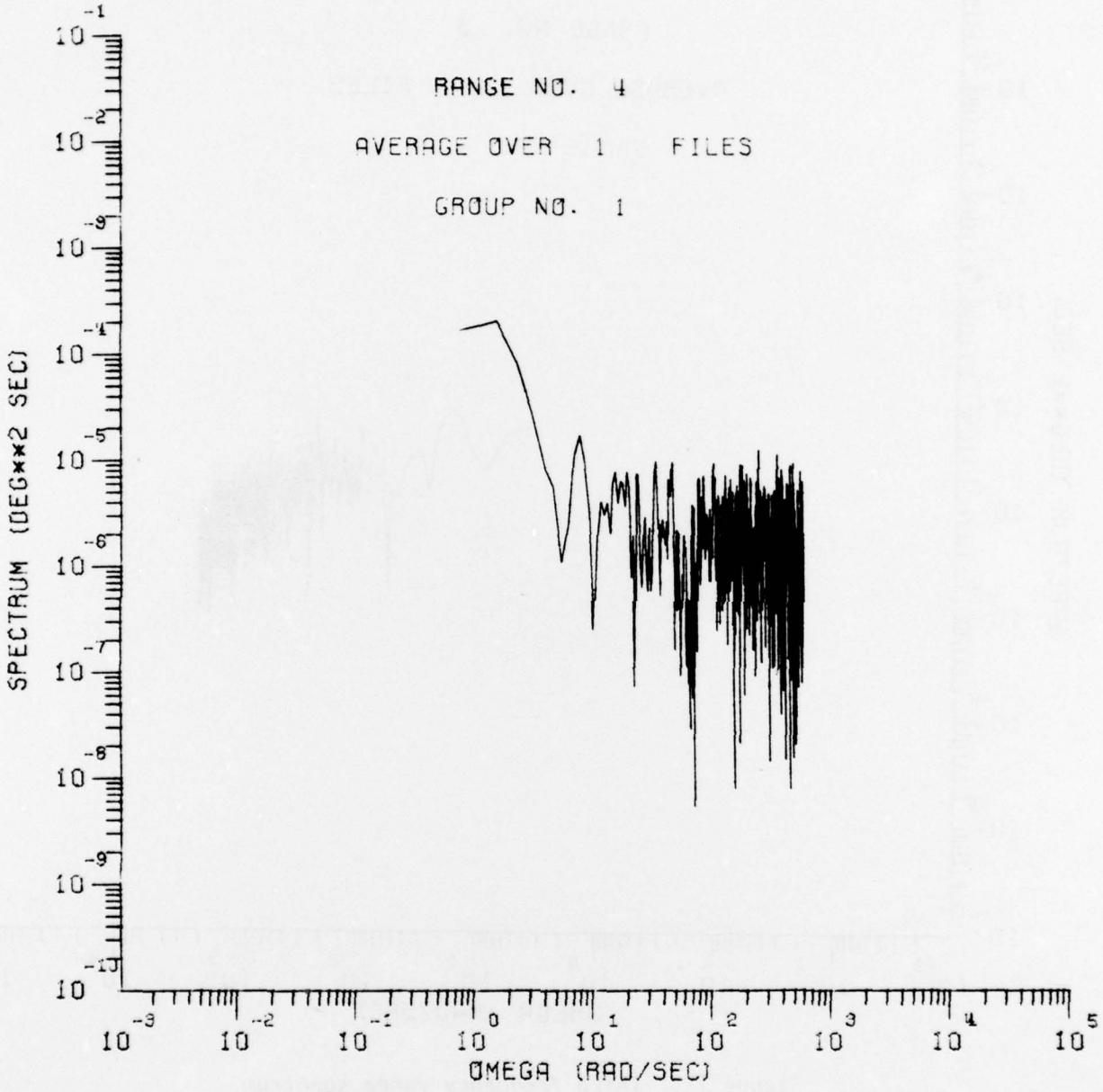

Figure 12. Fourth frequency range spectrum.

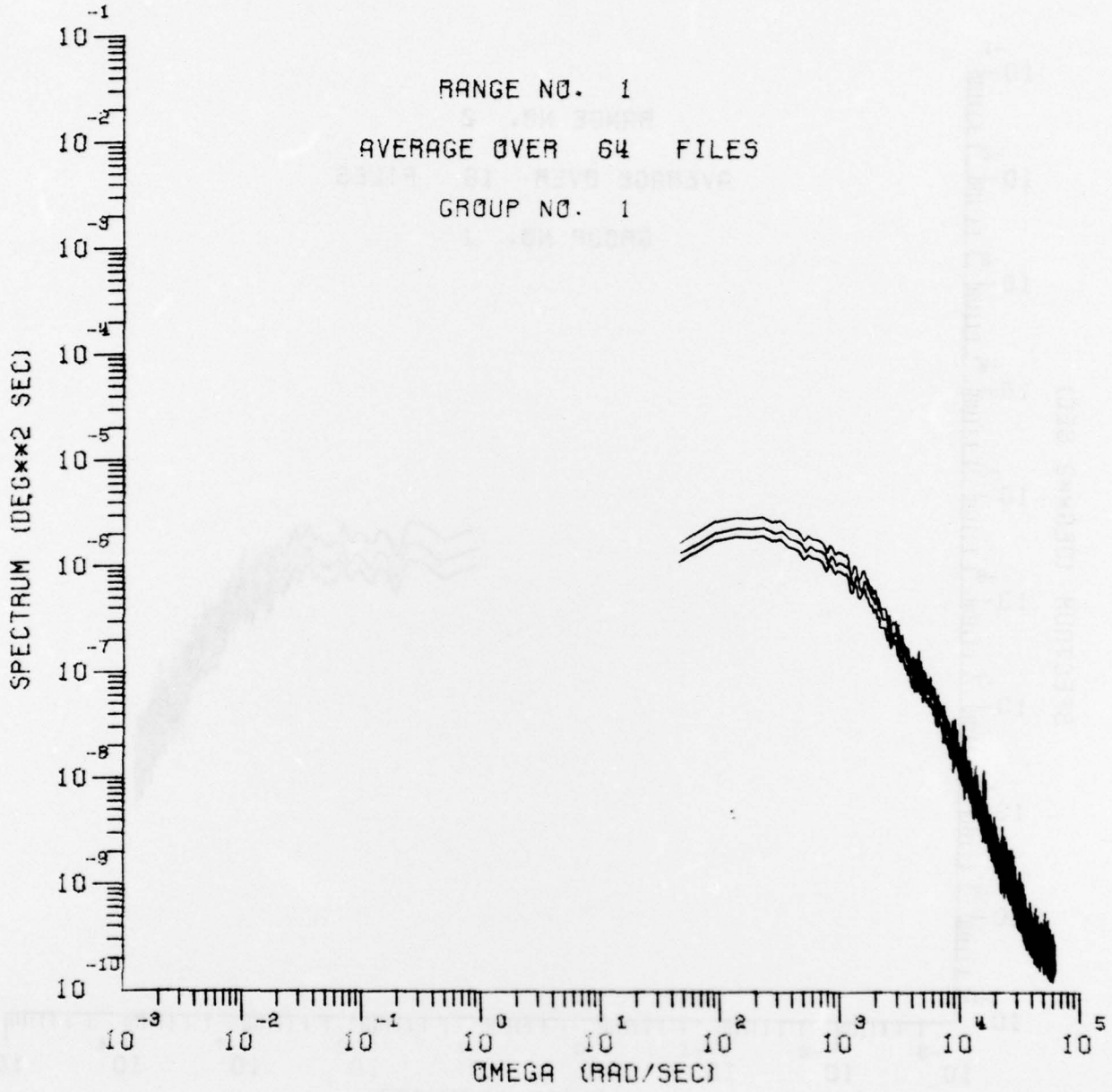

Figure 13. Spectrum with 90% confidence interval.

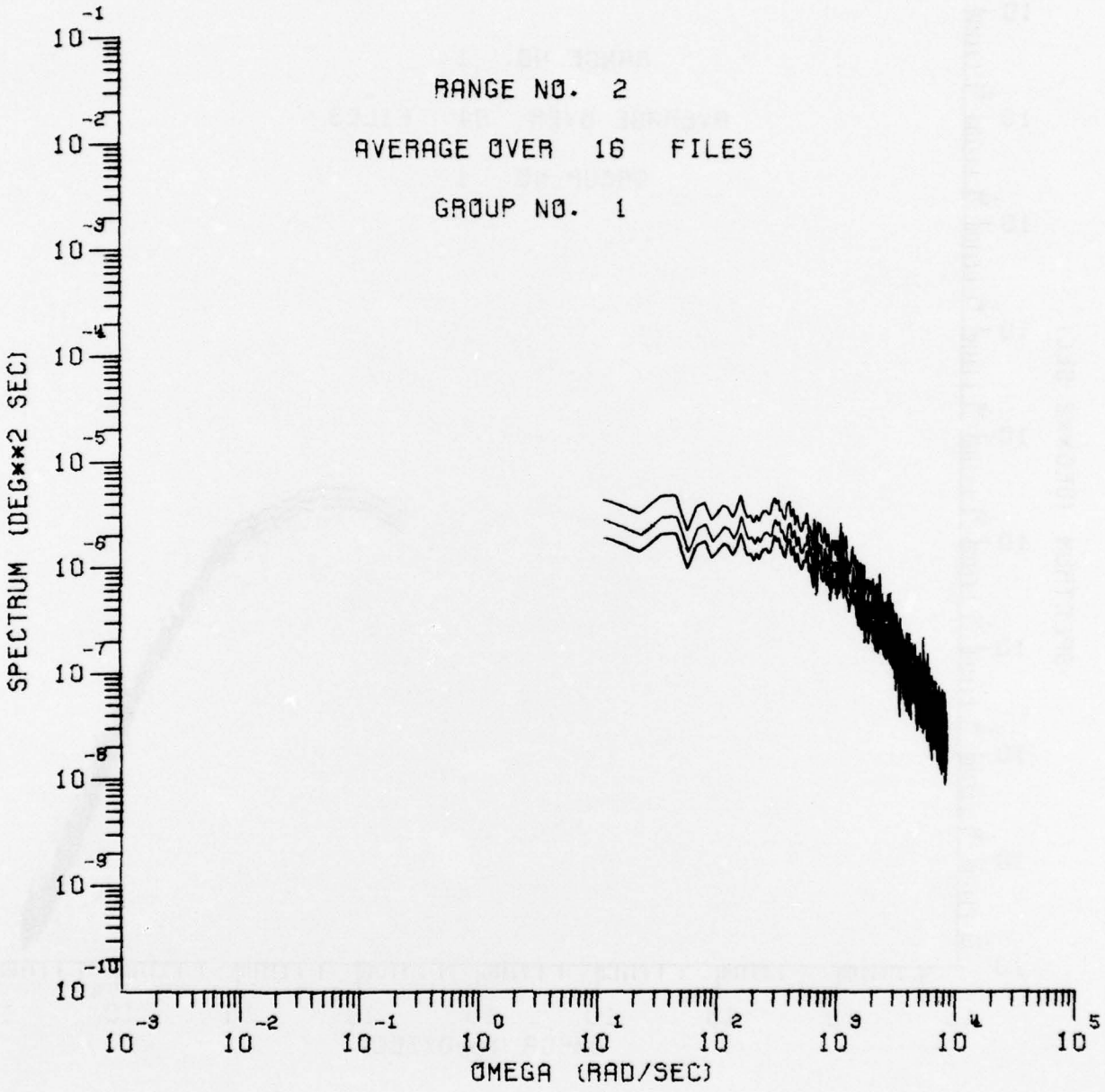

Figure 14. Spectrum with 90% confidence interval.

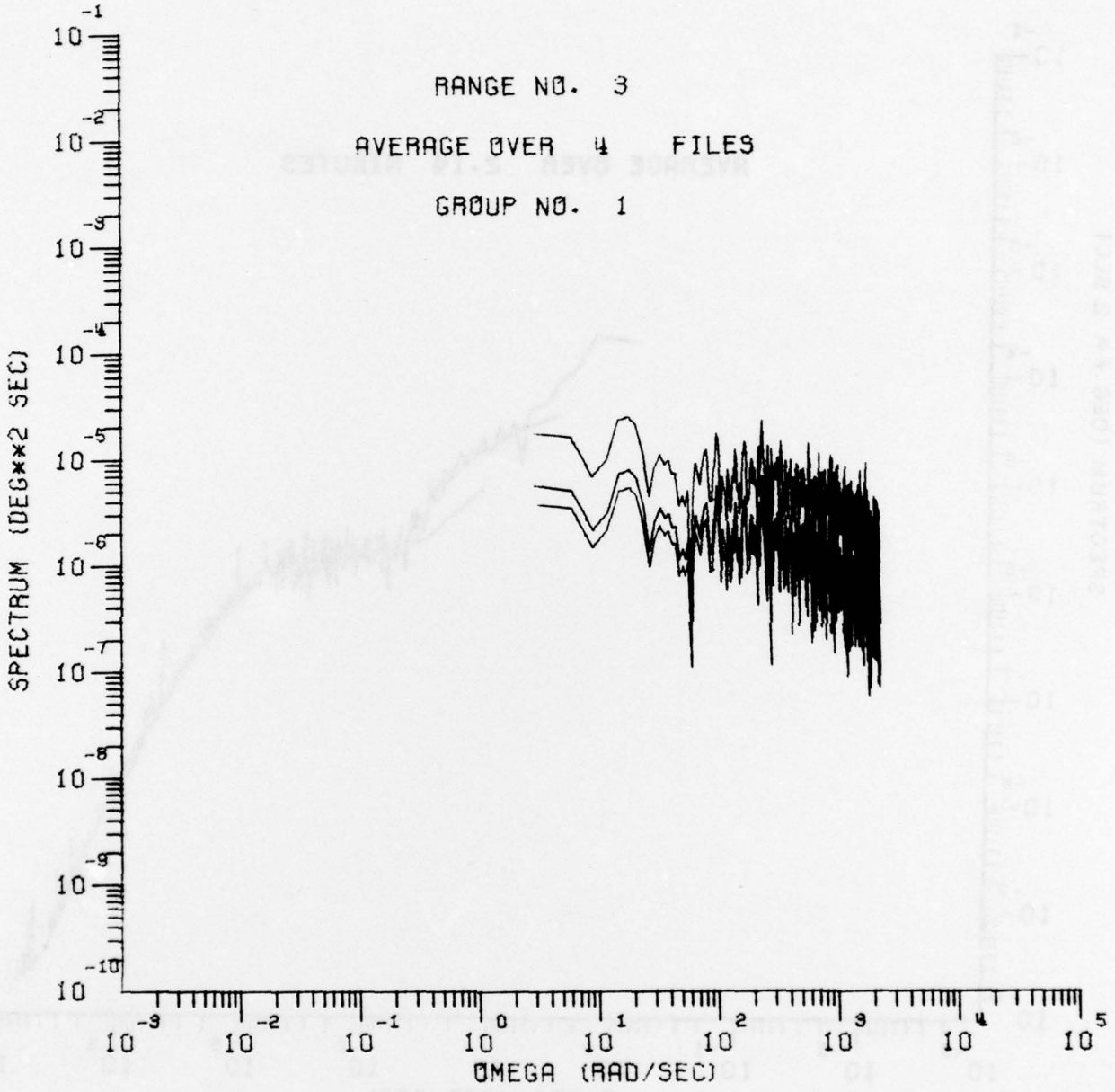

Figure 15. Spectrum with 90% confidence interval.

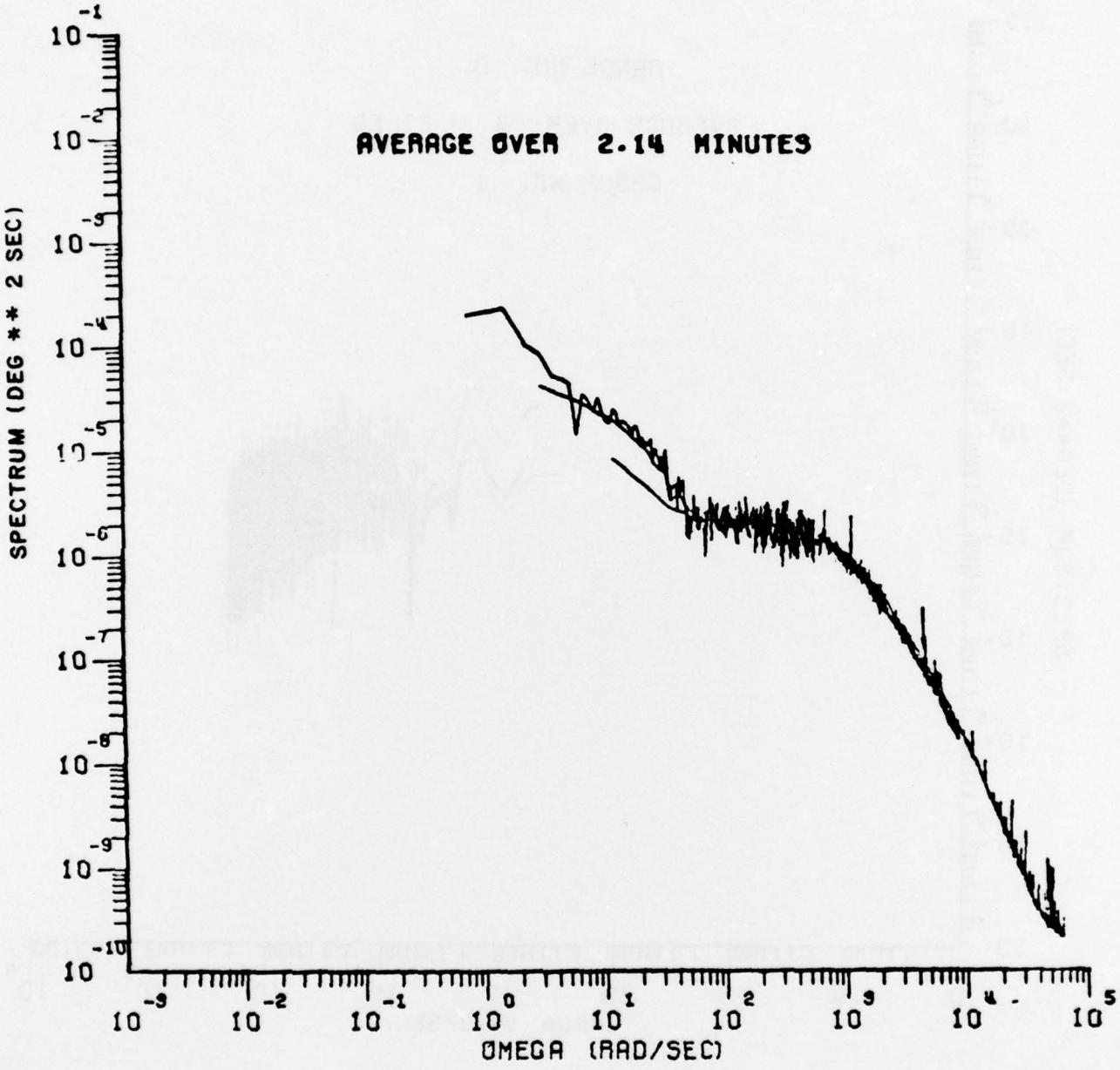

Figure 16-a. Composite of all frequency ranges averaged over 2.14 minutes.

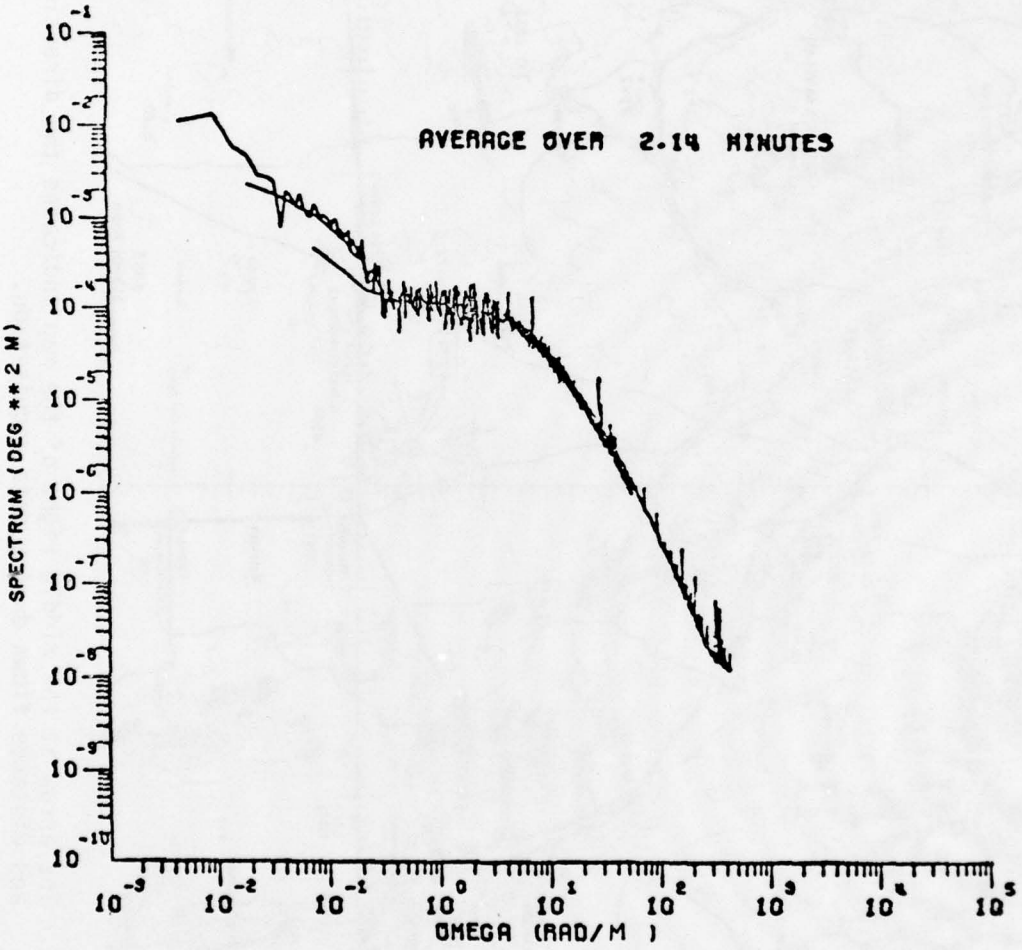

Figure 16-b. Spatial spectrum corresponding to Figure 15-a (velocity = 155 m/sec.).

BEST AVAILABLE COPY

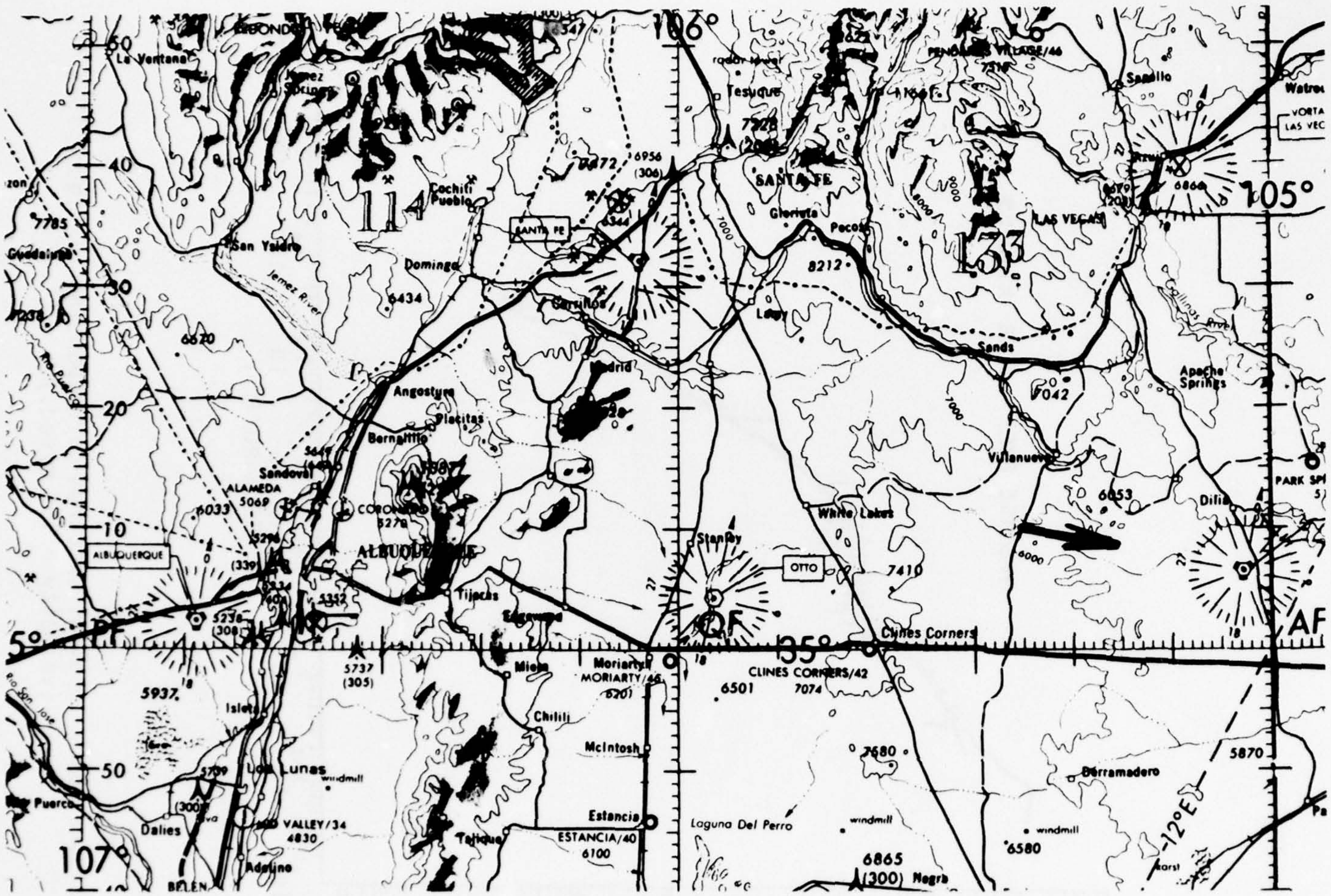

Figure 17. The arrow at the middle right of the map indicates the direction and distance flown during data acquisition.

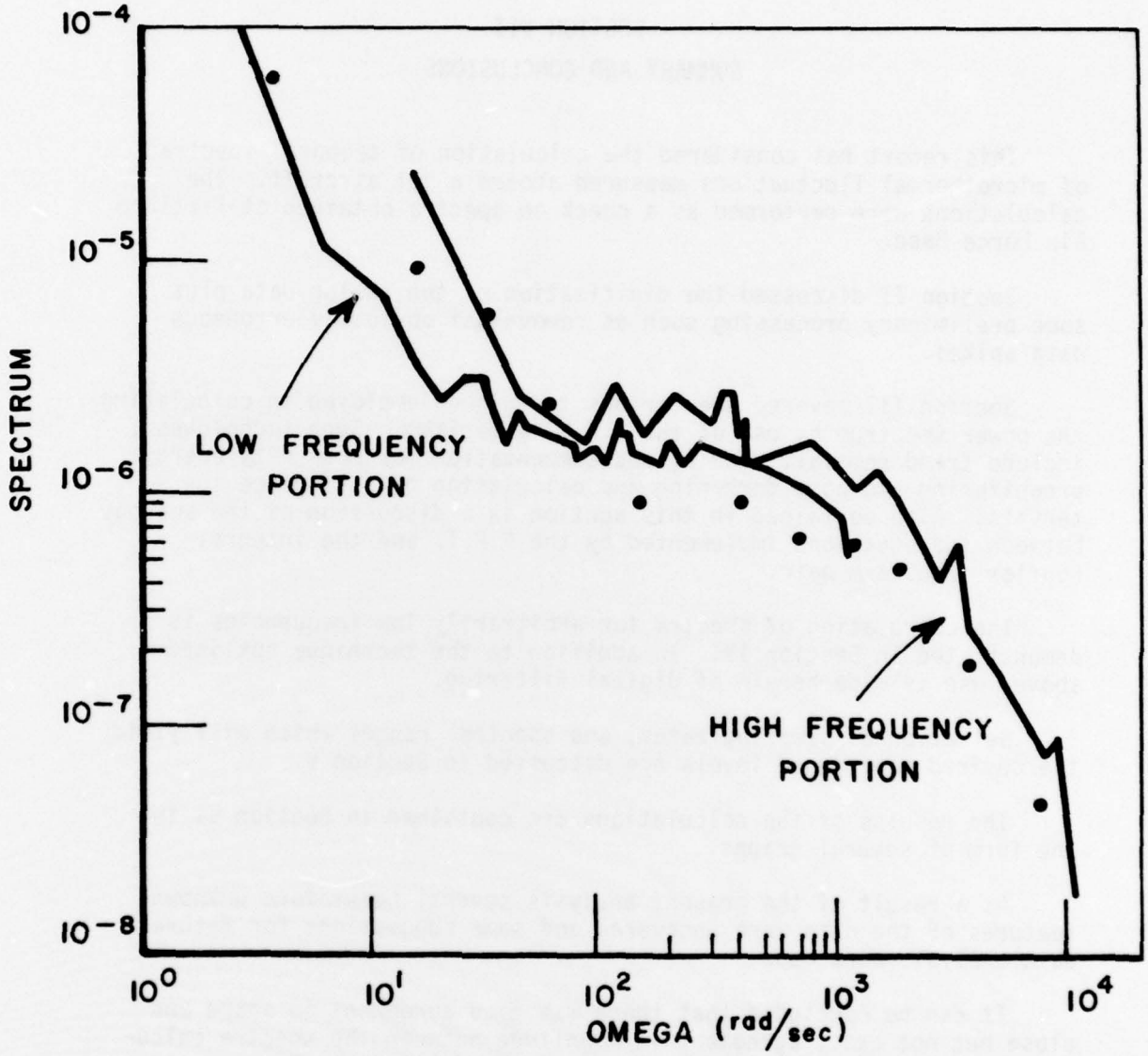

Figure 18. Comparison of spectrum calculated at Kirtland Air Force Base (solid lines) and the spectrum calculated herein (points).

SECTION VII

SUMMARY AND CONCLUSIONS

This report has considered the calculation of temporal spectra of microthermal fluctuations measured aboard a jet aircraft. The calculations were performed as a check on spectra obtained at Kirtland Air Force Base.

Section II discussed the digitization of the analog data plus some preliminary processing such as removal of obviously erroneous data spikes.

Section III covered the various techniques employed in calculating the power spectrum by use of the F.F.T. algorithm. Such techniques include trend removal, Hanning and compensation for non-unity energy, prewhitening and post darkening and calculation of confidence intervals. Also contained in this section is a discussion of the analogy between the equations implemented by the F.F.T. and the integral Fourier transform pair.

The calculation of spectra for arbitrarily low frequencies is demonstrated in Section IV. In addition to the technique outlined above, use is made herein of digital filtering.

Selection of sampling rates, and spectral ranges which will yield the desired confidence levels are discussed in Section V.

The results of the calculations are contained in Section VI in the form of several graphs.

As a result of the present analysis several heretofore unknown features of the data were uncovered and some suggestions for future data analysis were made.

It can be concluded that there was good agreement in shape and close but not exact agreement in magnitude between the spectra calculated herein and those calculated at Kirtland Air Force Base.

APPENDIX

In this appendix we demonstrate the decrease in relative energy experienced when a non-rectangular data window is employed. For the Hanning window the decrease is shown to be by a factor of 3/8.

The spectrum as expressed by Equation (1b) in the text is

$$C(K) = \frac{1}{N} \sum_{L=1}^{N} X(L) e^{-i \frac{2\pi}{N} (L-1)(K-1)} .$$

The total energy is thus given by

$$\sum_{K=1}^{N} |C(K)|^2 = \frac{1}{N^2} \sum_{K=1}^{N} \sum_{L=1}^{N} \sum_{M=1}^{N} X(L) e^{-i \frac{2\pi}{N} (L-1)(K-1)} X^*(M) e^{i \frac{2\pi}{N} (L-1)(M-1)}$$

$$= \frac{1}{N^2} \sum_{L=1}^{N} \sum_{M=1}^{N} X(L) X^*(M) \sum_{K=1}^{N} e^{-i \frac{2\pi}{N} (L-1)(K-M)}$$

$$= \frac{1}{N^2} \sum_{L=1}^{N} \sum_{M=1}^{N} X(L) X^*(M) [N \delta_{K,M}]$$

Then

$$E \equiv \sum_{K=1}^{N} |C(K)|^2 = \frac{1}{N} \sum_{L=1}^{N} |X(L)|^2 .$$

For the rectangular data window the relative energy is ($X(L)=1$; $L=1,2,\cdots,N$)

$$E_R = \frac{1}{N} \sum_{L=1}^{N} 1 = 1.$$

Now the Hanning window as expressed by Equation (14) in the text is

$$X(L) = \frac{1}{2} \left[1 + \cos \frac{(L-1-N/2)\pi}{N/2} \right] .$$

And the relative energy is

$$E_H = \frac{1}{4N} \sum_{L=1}^{N} \left[1 + \cos \frac{(L-1-N/2)\pi}{N/2}\right]^2$$

$$= \frac{1}{4N} \sum_{L=1}^{N} \left[1 + 2\cos \frac{(L-1-N/2)\pi}{N/2} + \cos^2 \frac{(L-1-N/2)\pi}{N/2}\right]$$

$$= \frac{1}{4N} \sum_{L=1}^{N} 1 + \frac{1}{2N} \sum_{L=1}^{N} \left[\frac{e^{i\frac{2\pi}{N}(L-1-N/2)} + e^{-i\frac{2\pi}{N}(L-1-N/2)}}{2}\right]$$

$$+ \frac{1}{4N} \sum_{L=1}^{N} \left[\frac{e^{i\frac{4\pi}{N}(L-1-N/2)} + 2 + e^{-i\frac{4\pi}{N}(L-1-N/2)}}{4}\right]$$

$$= + \frac{1}{4} - \frac{1}{4N} \sum_{L=1}^{N} e^{i\frac{2\pi}{N}(L-1)} - \frac{1}{4N} \sum_{L=1}^{N} e^{-i\frac{2\pi}{N}(L-1)}$$

$$+ \frac{1}{16N} \sum_{L=1}^{N} e^{i\frac{4\pi}{N}(L-1)} + \frac{1}{8} + \frac{1}{16N} \sum_{L=1}^{N} e^{-i\frac{4\pi}{N}(L-1)}$$

$$E_H = \frac{1}{4} + \frac{1}{8} = \frac{3}{8}$$

Q.E.D.

REFERENCES

1. Draper, N. R. and Smith, H., Applied Regression Analysis, John Wiley and Sons, 1966.

2. Bingham, C., Godfrey, M. D., and Tukey, J. W., "Modern Techniques of Power Spectral Estimation," IEEE Transactions on Audio and Electro-Acoustics, Vol. AU-15, No. 2, 6/67.

3. Welch, P. D., "The Use of Fast Fourier Transform for the Estimation of Power Spectra: A Method Based on Time Averaging Over Short, Modified Periodograms," IEEE Transactions on Audio and Electroacoustics, Vol. AU-15, No. 2, 6/67.

4. Blackman, R. B. and Tukey, J. W., The Measurement of Power Spectra: From the Point of View of Communications Engineering, Dover 1959.

5. Bendat, J. S. and Piersol, A. G., Random Data: Analysis and Measurement Procedures, Wiley-Interscience, 1971.

6. Hogg, R. V. and Craig, A. T., Introduction to Mathematical Statistics, 3rd Ed., The Macmillan Co., 1970.

7. Brigham, E. O., The Fast Fourier Transform, Prentice-Hall, 1974.

8. Bergland, G. D., "A Guided Tour of the Fast Fourier Transform," IEE Spectrum, Vol. 6, No. 7, 7/69.

9. Tukey, J. W., "An Introduction to the Calculations of Numerical Spectrum Analysis".

METRIC SYSTEM

BASE UNITS:

Quantity	Unit	SI Symbol	Formula
length	metre	m	...
mass	kilogram	kg	...
time	second	s	...
electric current	ampere	A	...
thermodynamic temperature	kelvin	K	...
amount of substance	mole	mol	...
luminous intensity	candela	cd	...

SUPPLEMENTARY UNITS:

plane angle	radian	rad	...
solid angle	steradian	sr	...

DERIVED UNITS:

Acceleration	metre per second squared	...	m/s
activity (of a radioactive source)	disintegration per second	...	(disintegration)/s
angular acceleration	radian per second squared	...	rad/s
angular velocity	radian per second	...	rad/s
area	square metre	...	m
density	kilogram per cubic metre	...	kg/m
electric capacitance	farad	F	A·s/V
electrical conductance	siemens	S	A/V
electric field strength	volt per metre	...	V/m
electric inductance	henry	H	V·s/A
electric potential difference	volt	V	W/A
electric resistance	ohm		V/A
electromotive force	volt	V	W/A
energy	joule	J	N·m
entropy	joule per kelvin	...	J/K
force	newton	N	kg·m/s
frequency	hertz	Hz	(cycle)/s
illuminance	lux	lx	lm/m
luminance	candela per square metre	...	cd/m
luminous flux	lumen	lm	cd·sr
magnetic field strength	ampere per metre	...	A/m
magnetic flux	weber	Wb	V·s
magnetic flux density	tesla	T	Wb/m
magnetomotive force	ampere	A	...
power	watt	W	J/s
pressure	pascal	Pa	N/m
quantity of electricity	coulomb	C	A·s
quantity of heat	joule	J	N·m
radiant intensity	watt per steradian	...	W/sr
specific heat	joule per kilogram-kelvin	...	J/kg·K
stress	pascal	Pa	N/m
thermal conductivity	watt per metre-kelvin	...	W/m·K
velocity	metre per second	...	m/s
viscosity, dynamic	pascal-second	...	Pa·s
viscosity, kinematic	square metre per second	...	m/s
voltage	volt	V	W/A
volume	cubic metre	...	m
wavenumber	reciprocal metre	...	(wave)/m
work	joule	J	N·m

SI PREFIXES:

Multiplication Factors	Prefix	SI Symbol
1 000 000 000 000 = 10^{12}	tera	T
1 000 000 000 = 10^{9}	giga	G
1 000 000 = 10^{6}	mega	M
1 000 = 10^{3}	kilo	k
100 = 10^{2}	hecto*	h
10 = 10^{1}	deka*	da
0.1 = 10^{-1}	deci*	d
0.01 = 10^{-2}	centi*	c
0.001 = 10^{-3}	milli	m
0.000 001 = 10^{-6}	micro	μ
0.000 000 001 = 10^{-9}	nano	n
0.000 000 000 001 = 10^{-12}	pico	p
0.000 000 000 000 001 = 10^{-15}	femto	f
0.000 000 000 000 000 001 = 10^{-18}	atto	a

* To be avoided where possible.

•U.S. GOVERNMENT PRINTING OFFICE: 1977-714-025/176